Controls of the global overturning circulation of the ocean

Article

CentAUR

Central Archive at the University of Reading

Reading's research outputs online

Review

Controls of the global overturning circulation of the ocean

Check for updates

Fabien Roquet[1] ✉, Michael J. Bell[2], Agatha M. de Boer[3], David Ferreira[4], C. Spencer Jones[5], Joseph H. LaCasce[6], Casimir de Lavergne[7], David P. Marshall[8], David R. Munday[9], Jonas Nycander[10] & Malin Ödalen[11]

The global overturning circulation (GOC) is the largest scale component of the ocean circulation, associated with a global redistribution of key tracers such as heat and carbon. The GOC generates decadal to millennial climate variability, and will determine much of the long-term response to anthropogenic climate perturbations. This review aims at providing an overview of the main controls of the GOC. By controls, we mean processes affecting the overturning structure and variability. We distinguish three main controls: mechanical mixing, convection, and wind pumping. Geography provides an additional control on geological timescales. An important emphasis of this review is to present how the different controls interact with each other to produce an overturning flow, making this review relevant to the study of past, present and future climates as well as to exoplanets' oceans.

The global overturning circulation (GOC) is responsible for the ventilation of deep and bottom water masses on decadal to millennial timescales. By connecting water masses from all four major basins across the full depth of the ocean (Fig. 1), it induces a large-scale redistribution of heat, carbon and nutrients, which makes it central to the Earth's climate and biogeochemical cycles[1]. In the current context of a fast-paced forced climate change, there are worries that the GOC could be modified in some fundamental ways[2–4], with long-term consequences for the Earth's climate[5–9]. Yet too little is known about what controls the GOC structure and intensity to reliably predict its potential response.

Knowledge about the GOC heavily relies on general circulation models, owing to the difficulty of observing a global system that varies on such a wide range of timescales. Despite their numerous limitations, models have given us a better idea of how the GOC may have looked in the past, and how it may change in the future. The "conveyor belt" picture[10], which represents the meridional circulation as a laminar flow following a well-defined pathway, has proved over-simplistic and is now replaced by a complex set of intricate current systems, full of eddies and varying on all timescales[11]. In this modern picture, the open geometry of the Southern Ocean plays a central role in determining the GOC[12].

The focus here is to present an overview of the different factors that shape the GOC. Disentangling the mechanisms responsible for the maintenance of overturning cells in the ocean has proved surprisingly difficult.

Unlike the atmosphere, which is warmed from below and cooled from above, the ocean is both warmed and cooled at the surface, i.e., at roughly the same geopotential level, a rather inefficient configuration to produce energetic overturnings as illustrated in the pioneering experiments of Sandström[13]. Mechanical sources of energy are required to explain the strength and structure of the GOC[14,15], while the convection generated by surface buoyancy fluxes acts as a net sink of mechanical energy. This has led many authors to conclude that the overturning circulation is "driven" by wind and tides, but not by surface buoyancy fluxes[16–18]. This conclusion arises when defining "drivers" uniquely as "power sources"[18]. We believe that this interpretation has brought unnecessary confusion in the literature and should be avoided in the future[19]. In fact, it is established that surface buoyancy fluxes have a strong impact on the GOC[20]. Clearly, the GOC as we observe it depends on both mechanical and buoyancy forcings acting together.

We propose here to carefully distinguish between the concepts of power source, control, and driver. An analogy with cars may be useful to illustrate the fundamental differences. The car is powered by gas combustion or electrical batteries. It is controlled by a steering wheel and the throttle and braking pedals. The driver is the operator of the car, most often a human acting with intent. What would be the equivalents for the ocean circulation? Winds and tides provide mechanical power sources, while the buoyancy forcing provides both sources and sinks of potential energy. The mixing,

[1]Department of Marine Sciences, University of Gothenburg, Gothenburg, Sweden. [2]Met Office, Exeter, UK. [3]Department of Geological Sciences and Bolin Centre for Climate Research, Stockholm University, Stockholm, Sweden. [4]Department of Meteorology, University of Reading, Reading, UK. [5]Department of Oceanography, Texas A&M University, College Station, TX, USA. [6]Department of Geosciences, University of Oslo, Oslo, Norway. [7]LOCEAN Laboratory, Sorbonne University-CNRS-IRD-MNHN, Paris, France. [8]Department of Physics, University of Oxford, Oxford, UK. [9]British Antarctic Survey, Cambridge, UK. [10]Department of Meteorology and Bolin Centre for Climate Research, Stockholm University, Stockholm, Sweden. [11]Climate and Environment Division, NORCE, and Bjerknes Centre for Climate Research, Bergen, Norway. ✉e-mail: fabien.roquet@gu.se

Fig. 1 | Global residual meridional overturning streamfunction. Observationally-constrained estimate based on the Estimating the Circulation and Climate of the Ocean version 4 release 4 (ECCOv4r4) reanalysis product[40], computed in **a** depth coordinate and **b** density coordinate (based on potential density σ_2). The contour interval is 10 Sv (1 Sv = 10^6 m^3 s^{-1}). Zonal mean density contours are indicated (thin dashed black curves) on the depth-coordinate streamfunction. Similarly, zonal mean depth contours are shown on the density-coordinate streamfunction. Residual streamfunctions include the Eulerian and bolus (eddy-induced) components of the flow which advect tracers. Two major cells structure the present overturning circulation, an upper cell exchanging properties between the North Atlantic and the Southern Ocean, referred to as the AMOC, and a lower cell associated with the circulation and transformation of Antarctic Bottom Water (AABW)[185]. These cells interact in a number of ways and are thought to be connected in a global figure-of-eight structure[186]. Both the upper and lower overturning cells reach the surface in the Southern Ocean, making it an important place for the global climate. In addition, shallow tropical cells contribute to a large heat transport at low latitudes[187,188]. The two streamfunctions provide broadly similar pictures, except in the Southern Ocean where a strong Deacon cell present in the depth space is absent from the density space[42]. The ECCOv4r4 product is a physically-consistent reconstruction of the ocean state on a 1° global grid for the period 1992–2017. It was created using an ocean model that assimilates a large number of observations from across this time period. It is presented as an illustration of the GOC structure and pathways, yet it is associated with many uncertainties and biases[189] and should therefore be considered critically.
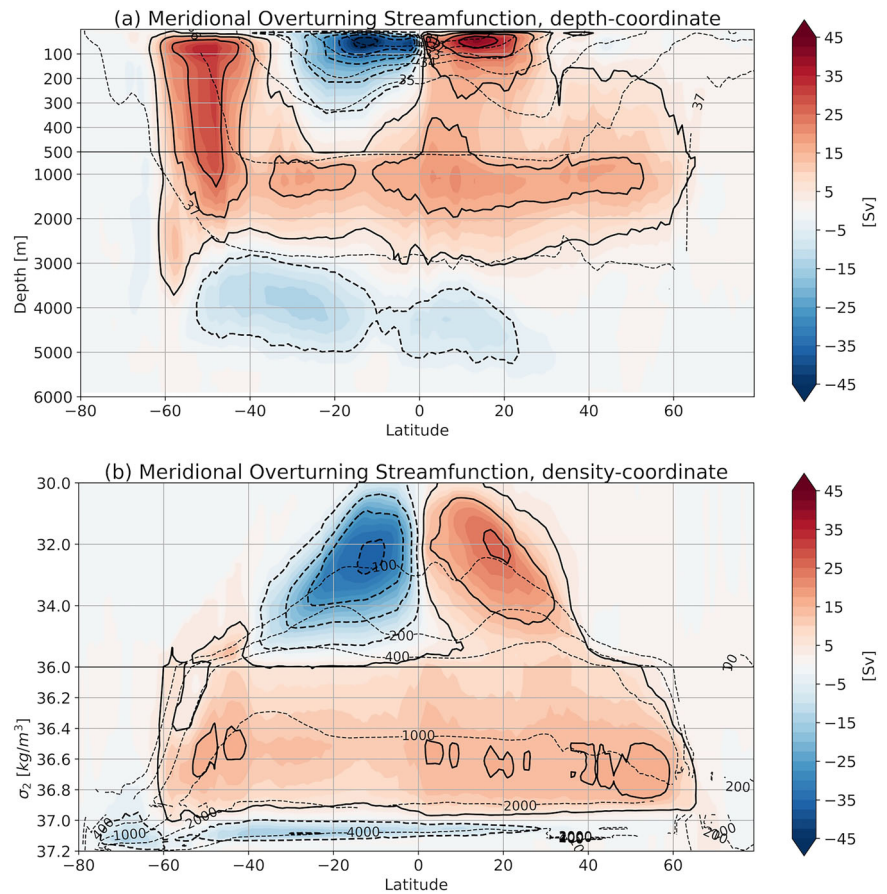
pumping, and convection that these forcings induce control the flow (Fig. 2). The ocean has no (known) driver, suggesting that this term should be abandoned—or at least used with great caution.

In this review, we will focus on controls, seen as processes that affect the shape, magnitude, and variability of the overturning flow through the modulation of external forcings. Considerations of the energy budget will be our starting point, as the importance of a given control can be judged by its ability to supply or remove energy. Sinks and sources of energy are equally important: the balance between the two determines the steady state. Section "Energetics of overturning circulations" presents the energetics of overturning circulations and discusses the horizontal convection regime (surface buoyancy forcing only, illustrated in Fig. 3a).

The rest of the review is organized to gradually introduce the different types of control that are illustrated in Fig. 3. Our goal here is not to cover all combinations of wind, mixing, and geometry, but to provide a framework for understanding the GOC as we observe it. In section "Buoyancy driven circulations: convection + mechanical mixing", we consider the buoyancy forcing with convection and mixing (buoyancy-driven circulation, Fig. 3b). We then add the effect of wind pumping in section "Adding wind pumping to the picture" (Fig. 3c for a closed basin, and Fig. 3d in the presence of a circumpolar gateway), which is most relevant in the presence of a stratification. Note that this stratification requires buoyancy forcing and mixing to exist in the first place. Section "Geographic controls", which discusses geographic controls acting on geological scales, highlights the importance of the continental boundaries, bathymetry constraints and orography. Finally, section "Conclusion" summarizes the main takeaway points and discusses future challenges.

Energetics of overturning circulations

The budget of mechanical energy (see Box 1) helps to elucidate the effects of various controls affecting the GOC. The ocean has large reservoirs of potential energy (~20 YJ, with 200–700 EJ available to the general circulation) and kinetic energy (~ 10 EJ as geostrophic flow)[21]. For these energy reservoirs to maintain ocean circulation/stratification, power must be continuously input to offset on-going energy dissipation. One difficulty in interpreting energy budgets comes from the wide range of spatial and temporal scales at which potential and kinetic energy are being converted back and forth. Integrating the entire range of scales produces a picture where wind and tides provide energy sources while viscous dissipation is a sink (Fig. 4a). The net effect of molecular diffusion (M_i in Fig. 4a) can either be a net source or sink depending on whether the average stratification is stable or not.

The energy budget for the time-mean large-scale circulation (typical of that simulated by coarse ocean models) produces a very different picture (Fig. 4b). In this picture, the potential energy budget becomes central, as it provides a link between the small-scale mixing and the mean circulation. The strength of this link depends on the turbulent diffusivity sustained by different mixing processes.

The total surface wind power input to the ocean is around 70 TW, much greater than the ~2–4 TW required to maintain the general circulation[21]. The extra power is primarily directed into surface gravity waves (~60–68 TW)[22], with a small residual feeding internal waves (<0.2 TW)[23]. Energy is also diverted into the ageostrophic circulation (~3 TW)[24], which is mostly dissipated in the mixed layer and is largely unable to contribute to mixing at depth[23,25]. Surface wind and waves generate vertical diffusivities in excess of 10^{-2} m^2 s^{-1} in the surface boundary layer[26]. If the

Fig. 2 | Illustration of the main relations existing between external forcings, controls and flow patterns. The global circulation is the resultant of all the different flows added together. The wind stress can affect the circulation in three main ways: (1) by producing mechanical mixing (together with tides), (2) by generating pumping, and (3) by modulating heat and freshwater (FW) fluxes. More indirectly, wind stress can enhance strong western boundary currents that affect the surface buoyancy fluxes through sea surface temperature (SST) advection. On the other hand, heat and freshwater fluxes produce high latitude convection, ventilating the deep ocean and maintaining a deep stratification. The relative importance of different controls depends on the time and spatial scales under consideration, ranging from seasonal to multi-centennial. For example, winds and the surface buoyancy forcing are more relevant than interior mixing in driving interannual to decadal variability, however, long adjustment time scales depend more on interior mixing.
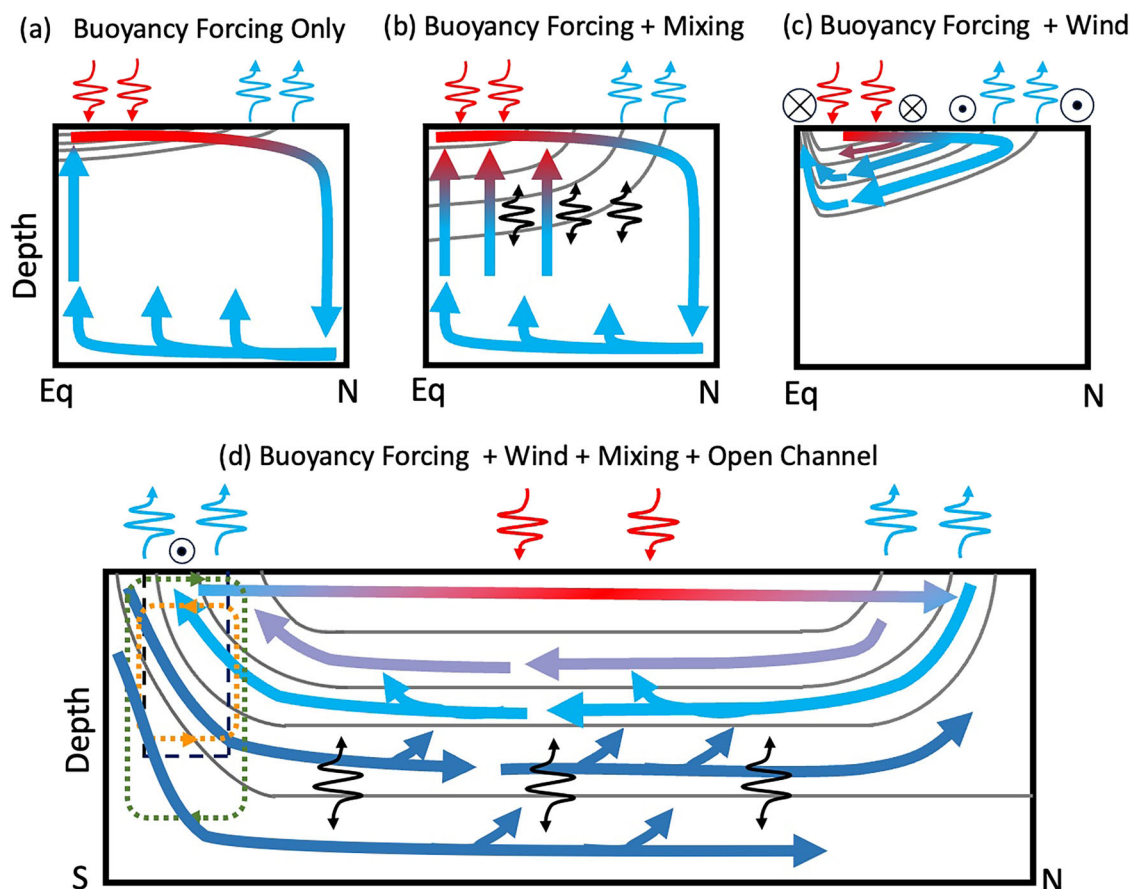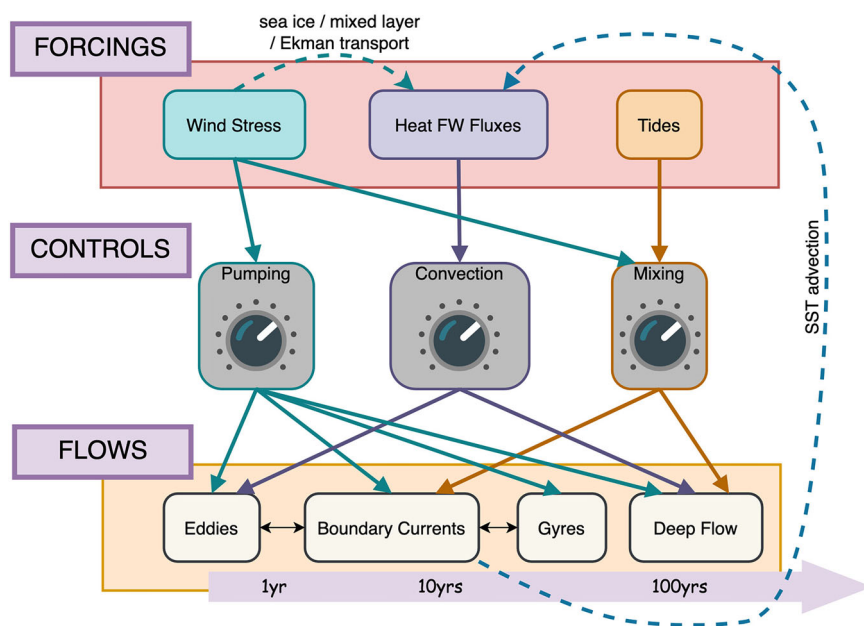
Fig. 3 | Schematic showing four different scenarios. a Buoyancy forcing applied at the surface. This configuration corresponds to the horizontal convection regime, where mixing is solely generated by flow instabilities. **b** Buoyancy forcing and mechanical mixing, producing a deeper stratification and a stronger overturning circulation. **c** Buoyancy forcing and surface winds, in a configuration that resembles tropical cells. In this configuration, wind-driven Ekman pumping maintains a deeper thermocline and the interior flow is largely adiabatic. **d** Combined buoyancy forcing, wind and mixing, in the presence of a circumpolar gateway (black dashed line). The green dotted line represents the Ekman circulation cell and the orange dotted line represents the circulation induced by eddies across the open channel. This configuration bears much resemblance with the present-day deep and bottom overturning circulation.

Box 1 | Budget equations for mechanical energy (Fig. 4a)

The gravitational potential energy for the Boussinesq equations with a linear equation of state is defined by:

$$U = g \int z\rho \, dV, \tag{5}$$

where ρ is the in situ density, and z is the height relative to the sea surface. Here and below, the integral is over the entire ocean volume. The kinetic energy is:

$$K = \frac{1}{2} \int \rho_0 |\mathbf{v}|^2 \, dV, \tag{6}$$

where $\mathbf{v}$ is the velocity, and ρ_0 a constant reference density. The energy equations are:

$$\frac{dU}{dt} = M_i - C, \tag{7}$$

$$\frac{dK}{dt} = W + \Phi + C - D. \tag{8}$$

Equations (7) and (8) are illustrated in Fig. 4a. D is the viscous dissipation

(which is positive definite), W the forcing by surface wind stress τ, and Φ the tidal forcing. The conversion (C) from potential to kinetic energy can be obtained from two different but equivalent expressions (through integration by parts). The first one is written in terms of the vertical velocity w, and the second one in terms of the diapycnal velocity:

$$C = -g \int w\rho \, dV = g \int z\mathbf{v} \cdot \nabla \rho \, dV. \tag{9}$$

The effect of interior vertical mixing is given by:

$$M_i = -g \int \kappa \frac{\partial \rho}{\partial z} \, dV = \rho_0 \int \kappa N^2 \, dV, \tag{10}$$

where κ is the molecular diffusivity and N is the buoyancy frequency. We have neglected penetrative solar heating and geothermal heating and assumed that the surface buoyancy flux occurs at $z = 0$. Hence, this flux does not directly affect the potential energy. However, it is key in generating the vertical density gradients onto which mixing can act. We stress that a complete energy budget should be based on a nonlinear equation of state to include important processes such as cabbeling or thermobaricity[190,191].

stratification is stable, mixing converts small-scale turbulence to potential energy. If it is unstable, convection enhances diffusivity to very large values, acting as a net sink of potential energy (~0.24 TW[27]).

The breaking of internal waves, in part generated by flow over sharp bathymetry near the seabed, is among the most important sources of interior turbulence[28]. These waves can propagate long distances prior to breaking, leading to a complex geography of mixing[29]. About 1 TW of tidal energy is powering the internal wave field in the open ocean (the remaining ~2 TW are dissipated in shelf seas)[30–32]. It is likely that it is more than enough to sustain the deep stratification[33]. Only about 0.3 TW of the tidal power input to internal waves ultimately dissipates and causes mixing in the deep (>1 km) ocean[34]. Tidal and wind-driven internal waves combined with geothermal heating and mixing in deep overflows/throughflows enhance diffusivity near the seafloor, to values $>10^{-4}$ m^2 s^{-1}, with much smaller values in the interior ocean[35], typically $<10^{-5}$ m^2 s^{-1}—still significantly larger than the molecular thermal diffusivity of ~10^{-7} m^2 s^{-1}.

A remaining fraction of wind power input of ~0.6 TW enters the mean geostrophic interior, with more than two thirds in the Southern Ocean[36]. This energy is converted to mean potential energy through Ekman pumping, then converted to eddy kinetic energy through baroclinic instability[37]. The generation of mesoscale eddies is a primary energy pathway, parameterized in non-eddying ocean models as a density thickness diffusion or equivalent[38].

Depth-density streamfunctions

To move beyond global estimates, the energetics of the GOC can be displayed with the streamfunction in density-depth coordinates, $\psi(\rho, z)$, defined as the upward volume flux through the horizontal surface at depth z with density smaller than ρ[39]. This representation of the overturning focuses on the diapycnal flow, while adiabatic circulation is invisible. It can be shown that the conversion C from potential to kinetic energy is given by the integral of $\psi(\rho, z)$ over the (ρ, z)-plane:

$$C = \int \psi(\rho, z) \, d\rho dz. \tag{1}$$

Equation (1) shows that C is given by the product of the depth range, the buoyancy range and the diapycnal volume transport. The sign of C in an overturning cell determines the type of circulation. If the upwelling water is denser than the downwelling water (such circulation is often called thermally indirect, or mechanically forced), the circulation on the density-depth plane is counterclockwise. Then $\psi(\rho, z)$ and C are negative, i.e., kinetic energy is converted to potential energy. In contrast, a positive conversion (from potential to kinetic) is associated with a thermal direct cell upwelling light water and downwelling dense waterFigure 5 shows the density-depth streamfunction from the ocean state estimate ECCOv4r4[40], using potential density σ_2 instead of in situ density as the horizontal coordinate. Figure 5a shows the residual streamfunction $\psi(\sigma_2, z)$, which is the sum of the Eulerian (i.e., resolved) streamfunction ψ_E (Fig. 5b) and the eddy-induced (parameterized) streamfunction ψ_b (Fig. 5c). The eddy-induced streamfunction ψ_b, given by the Gent-McWilliams (GM) parameterization[38], flattens out isopycnal surfaces to mimic the effect of baroclinic instability, and is a sink of potential energy (thermally direct). As expected, ψ_E and ψ_b nearly cancel over a large part of the plane (Fig. 5b, c).

The GOC in ECCOv4r4 and other realistic ocean models consists of two main cells, a deep and a bottom one (Fig. 1). In the bottom cell, very dense Antarctic Bottom Water (AABW) is formed near Antarctica through a combination of convection and deep overflows. This AABW flows northward and is gradually lightened by mixing and geothermal heating, thereby upwelling across isopycnals, which means that the circulation is thermally direct (C is positive). In density-depth coordinates, this cell corresponds to the thin red cells at $\sigma_2 > 37.0$ (Fig. 5a), in agreement with the density range of the blue bottom cell in depth-latitude space (Fig. 1b).

In the deep cell, dense North Atlantic Deep Water (NADW) is formed in the subpolar North Atlantic, flows southward at depths of 1–4 km, and finally upwells in the Southern Ocean. This cell has density mainly in $35 < \sigma_2 < 37.0$ in Fig. 1b (where it is red) and a (where it is blue). It is often regarded as wind-driven and mainly adiabatic[15,18], although mixing contributes as well[41]. It should then be very weak on the density-depth plane, with only a small density difference between the downwelling and upwelling water. This agrees with the very weak anticlockwise (blue) cell below 1000 m

(a) Full budget

(b) Mean large-scale budget
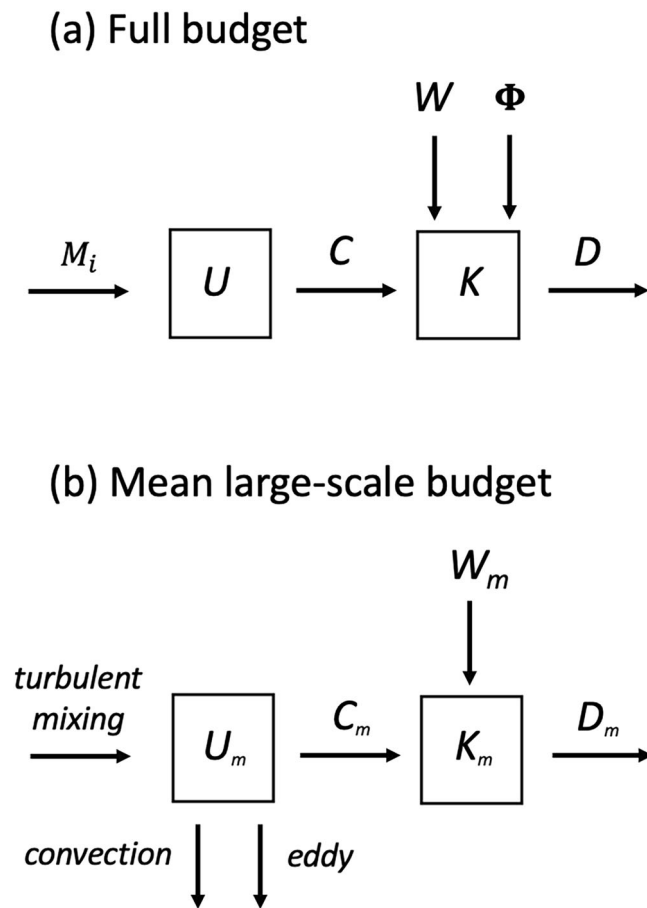
Fig. 4 | Diagrams of the ocean's mechanical energy budget. a Budget when all motion is resolved and described by the equations of motion, and **b** budget for the large-scale mean ocean state when small- to meso-scale motion is parameterized. In the former case, potential energy U is generated by molecular diffusion and converted (C) to kinetic energy K. Kinetic energy is also powered by wind (W) and tides (Φ) and eventually dissipated (D). The latter case **b** describes the mean large-scale budget for the mean potential energy U_m and mean kinetic energy K_m relevant to a non-eddying ocean model, with parameterized turbulent mixing acting as a source of mean potential energy, and convection and mesoscale eddy conversion acting as sinks. Wind work on the large-scale surface velocities (W_m) is either dissipated (mostly locally in the surface turbulent layer) or it powers the geostrophic circulation through Ekman pumping.

in Fig. 5a. A puzzling aspect is the densification (probably cooling) of the downwelling water along the indirect deep cell. It is not yet well understood what causes this densification, but it could be related to convection, cabbeling or some residual of the Deacon cell[42].

The integral over ψ_E gives a total conversion of 760 GW from kinetic to potential energy (i.e., C_m is negative in Fig. 4b), while the integral over ψ_b gives a potential energy sink of 860 GW. This shows that the main path of the energy transformation in this model begins with kinetic energy input by wind stress, continues with transfer to potential energy via Ekman pumping, and ends with the sink due to the eddy parameterization (which, crucially, is not associated with a transfer to eddy kinetic energy as in the real ocean). Since this parameterization is by definition adiabatic (except near the surface), it is natural that ψ_E and ψ_b nearly cancel out. Overall, energy transfers relevant to the GOC represent a tiny fraction of the full energy budget.

On the horizontal convection regime
Energy estimates demonstrate the dominance of wind and tides in providing energy to the general circulation. But one may wonder if the overturning circulation would be qualitatively similar in their absence. A well-known theorem about horizontal convection helps appreciating the differences. Horizontal convection is here defined as a circulation solely forced by the surface buoyancy fluxes (i.e., $W = 0$ and $\Phi = 0$, see Box 1), with a constant molecular diffusivity[43]. This circulation is illustrated in Fig. 3a.

At steady state, molecular diffusion must provide the source of energy through conversion of heat to potential energy, in order to balance dissipation ($M_i = C = D$). The product of the molecular diffusivity and the maximum buoyancy range therefore provides an upper bound on the total viscous dissipation (see Eq. (10)). This result, known as the Paparella-Young theorem[16], has been generalized to the case of a nonlinear equation of state with separate molecular diffusivities for temperature and salinity[44,45]. The upper bound obtained is 7.2 GW, which is significantly smaller than the ~100 GW estimated from ECCOv4r4 (Fig. 5), and orders of magnitude smaller than observed rates of dissipation. This demonstrates that most of the energy dissipated by viscosity must originate from external sources of mechanical energy: winds and tides.

As pointed out by several authors, the Paparella-Young theorem does not imply that the overturning circulation involved in horizontal convection must be weak[46,47]. Indeed, there is no direct connection between the viscous dissipation D and the strength of the overturning, and simulations show that horizontal convection can involve substantial overturning. However, the upper bound on dissipation also applies to the conversion C, which *is* closely related to the overturning.

The depth-density streamfunction helps to understand this constraint. The water mass transformation is towards lighter water ($\mathbf{v} \cdot \nabla \rho < 0$) at depth and towards denser water ($\mathbf{v} \cdot \nabla \rho > 0$) at the surface, so the circulation is clockwise in depth-density space, and $\psi(\rho, z)$ is positive. Since the interior is weakly stratified, with density close to that of the densest surface water, the streamfunction $\psi(\rho, z)$ has a very "thin" reversed-⅂ shape, with a small density range in the interior. Near the surface there is a wide range of buoyancy in a thin boundary layer (a few meters thick only). Even if the overturning (the magnitude of ψ) is large, Eq. (1) shows that conversion remains small, as required by the Paparella-Young theorem.

Buoyancy driven circulations: convection + mechanical mixing
We now consider the overturning generated by surface buoyancy forcing in the presence of mechanical mixing. Such flows have been referred to as "buoyancy driven circulations"[48]. This has introduced some confusion, as in reality mechanical mixing is powered by wind and tides, while the buoyancy forcing itself depends to leading order on the surface wind stress[49]. Similarly, "wind driven circulations" are strongly shaped by the buoyancy-forced stratification[50,51]. In fact, this terminology refers to a distinction between two ways to control the circulation: mixing (diffusion/convection) in the buoyancy driven case, and pumping in the wind driven case.

Simulations by general circulation models suggest that AMOC variability on decadal and longer timescales is dominated by changes in buoyancy forcing[52]. There are also indications that AMOC weakening following an increase in atmospheric CO_2 is mitigated by buoyancy changes, due to freshwater[53] and/or heat fluxes[54]. Thus, it is worth exploring what the ocean would look like without wind pumping. Mixing however is assumed to exist, either in the interior, near the boundaries or both. As noted earlier, substantial overturning and a deep thermocline can also exist even with weak mixing, depending on the basin geometry.

The concept of a "buoyancy-driven" overturning can be traced back to the late eighteenth and early nineteenth century, when sailors hypothesized that cold, sub-surface waters were likely of polar origin. The concept was put on firm theoretical ground in a series of works by Stommel et al.[55]. In these, the interior circulation is driven by uniform upwelling which balances convective downwelling in various locations and is linked by intense deep western boundary currents. One such deep current was discovered beneath the Gulf Stream shortly thereafter[56]. Diverse studies followed, both in the laboratory and numerically. Many were influenced by scaling relations linking the overturning and thermocline depth to the vertical diffusivity and large-scale buoyancy

Fig. 5 | Streamfunction in density-depth coordinates $\psi(\sigma_2, z)$ computed from ECCOv4r4, using potential density σ_2 as the density coordinate. The contour interval is 10 Sv. This streamfunction complements the more traditional depth-latitude and density-latitude streamfunctions featured in Fig. 1, giving a thermodynamic interpretation to the overturning circulation. Positive (red) ψ indicates clockwise circulation, where dense waters plunge and light waters upwell (thermally direct), and vice versa for thermally indirect cells. **a** Residual streamfunction ψ, obtained as the sum of **b** the Eulerian (resolved) streamfunction ψ_E and **c** the bolus (eddy-induced) streamfunction ψ_b. The vertical transport is obtained from the model output, and the corresponding diapycnal transport then obtained by assuming a circulation to be steady although not strictly true in ECCOv4r4[189]. The integral over the (σ_2, z)-plane is 100 GW for the residual streamfunction ψ. Separate cells can be distinguished, with 150 GW for the red tropical cell at $\sigma_2 < 36$, -100 GW for the blue deep cell, and 50 GW for the red bottom cell at $\sigma_2 > 36$. The total conversion can be further decomposed into the sum of **b** a net conversion from kinetic energy to potential energy of -760 GW for the Eulerian streamfunction ψ_E, and **c** a potential energy sink due to the GM eddy parameterization of 860 GW for ψ_b.
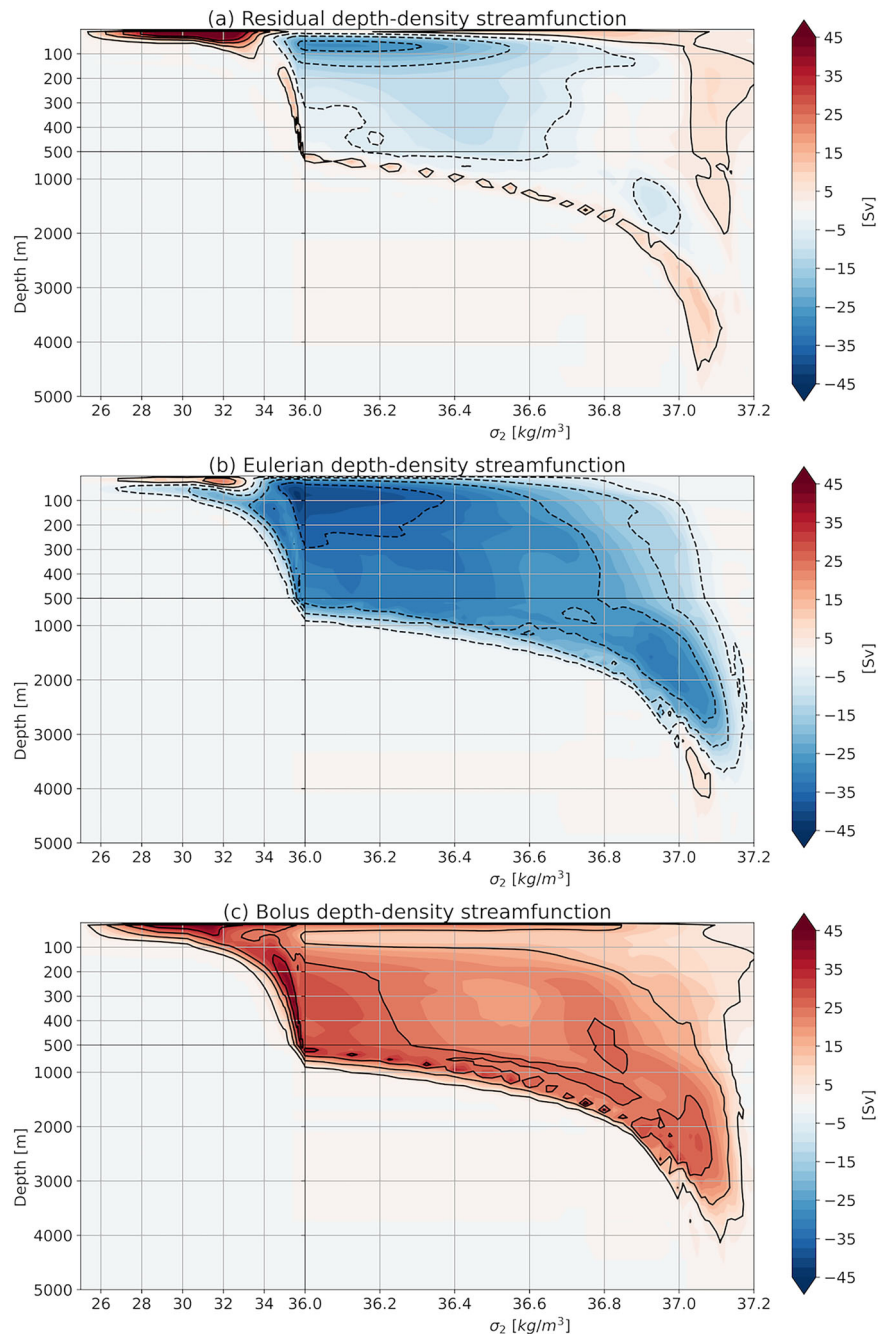
gradient. These stem from the geostrophic, hydrostatic, and continuity equations, combined with a simplified vertical advective-diffusive balance for buoyancy[57–59]. The resulting relations for the thermocline depth, h, and the overturning streamfunction, ψ, are:

$$h \sim \left(\frac{\kappa_v f^2 L}{\beta \triangle b}\right)^{1/3}, \quad \psi \sim \left(\frac{\kappa_v^2 \beta \triangle b}{f^2 L}\right)^{1/3} \quad (2)$$

where $\beta = df/dy$ is the meridional gradient of the Coriolis parameter, f, κ_v is the vertical turbulent diffusivity, $\triangle b = \max(b) - \min(b)$ is the large-scale buoyancy (b) difference in the domain and L is a horizontal basin scale[48,60,61]. The second relation predicts that overturning rates should increase with both diffusivity and surface buoyancy forcing, while the thermocline depth should increase with diffusivity but decrease with buoyancy forcing. Note that these scaling relations rest on

some drastic simplifications, such as the assumption that the meridional overturning transport scales with the zonal geostrophic transport[62]. Yet, they have proved surprisingly effective at predicting the broad characteristics of the overturning flow in a basin.

When matched to the observed thermocline depth and overturning, the scalings require a diffusivity of $\sim 10^{-4}$ m^2 s^{-1} [63], much larger than the $\sim 10^{-5}$ m^2 s^{-1} observed in the interior away from boundaries—the "missing mixing" conundrum that initiated much research since[14]. The discrepancy stems from multiple factors, all pointing to the necessity of considering a fully 3D description of the global circulation.

Failure of linear models and the importance of convection
Theoretical studies of the buoyancy driven circulation are based on the "planetary geostrophic equations" (also known as the thermocline equations[58]). These represent the simplest representation of basin-scale ocean dynamics. The flow is incompressible, hydrostatic and geostrophic,

except near the lateral boundaries where dissipation is required to satisfy no lateral flow. The only nonlinearity in the planetary geostrophic equations is in the buoyancy equation, due to horizontal and vertical advection. To solve the equations *analytically*, one must linearize the buoyancy equation, by assuming a uniform (and typically constant) mean stratification[64–67]. Alternatively, an ocean model solving the primitive equations can be used to solve the full nonlinear problem.

Comparing the linear and nonlinear solutions sheds light on the interior flows. The flow is generated by an imposed buoyancy gradient at the surface and is *zonal*. With buoyancy decreasing to the north, the thermal wind relation requires that the zonal velocity increases with height from the bottom, resulting in an eastward surface flow, both in nonlinear and linear solutions. Upon encountering the eastern boundary, the zonal flow splits northward and southward. The southward flow returns to feed the western boundary current, also in both solutions. In the linear model, the flow is westward also along the northern boundary. This effectively yields a double-gyre circulation, cyclonic in the north and anticyclonic in the south[68]. In contrast, the flow is *eastward* along the northern boundary in the nonlinear model, and the surface flow in the western boundary current is strictly to the north, yielding a single gyre[48].

The significant difference between the linear and nonlinear solutions is that convective mixing in the latter alters the stratification and greatly enhances downwelling in the north (Fig. 6). Convection occurs over a broad region in the north, but much of the sinking occurs near the eastern boundary, where lateral friction breaks geostrophy and permits large vertical velocities[67,69]. The mixed layer extends to the bottom, feeding a westward flow at the northern boundary beneath the eastward surface flow. In contrast, because the stratification is uniform and constant in the linear model, the flow is confined to the thermocline and the overturning is much weaker.

This illustrates the central importance of convection to produce an overturning circulation in physical space. But exactly how convection affects the circulation is rather indirect. Convection is not associated with any net mass transport[70], and the overturning is only weakly affected by the rate of convective adjustment[43,71]. Instead, convection sets the properties of the densest water, and dictates the depth of the overturning. The mixed layer may extend to the bottom, or overflows can form downstream of topographic sills to reach the deepest basins.

Sensitivity to turbulent diffusivity
An increase in interior mixing leads to an increase in the strength of the GOC[57,72,73]. Changing the mixing (through the prescribed background diffusivity) alters the supply of potential energy in a counter-intuitive way. Mixing raises the center of mass, all other things being kept constant. But stronger mixing changes the energy balance in such a way that increases overturning and deepens the pycnocline. The net result is a lowering of the center of mass of the water column, and an associated strengthening of the circulation[74]. Furthermore, stronger mixing can increase the overlap in density between the upper and lower overturning cells, which in turn can increase the connection between the Atlantic and Pacific basins and lead to a stronger GOC[75].

The changes are sometimes, but not always, consistent with the thermocline scalings (Eq. (2)). Diverse results indicate $\psi \sim \kappa_v^n$ with an exponent n equal to two-thirds as predicted by the scaling[48,72,76,77] or smaller[67,78,79]. Deviations could result from the surface restoring condition[78], the finite depth of deep convection[67], or from deviations from the assumption of a vertical advective-diffusive balance for buoyancy[79]. The overturning strength is also sensitive to whether diffusivity varies with the stratification, and several authors have argued that mixing energy rather than diffusivity should be kept constant in the scaling[80–82].

The strength and location of mixing impacts the distribution of upwelling. While some studies indicate a weak dependence on spatially-varying mixing[76], in others the spatial distribution of mixing is important for the overturning[83]. Interior upwelling is much reduced with realistically small vertical diffusivities, favoring the boundary currents[84,85]. Indeed, it is possible

that much of the GOC occurs near the boundaries, leading to a "pipe-like" circulation[86,87].

Numerical ocean models are useful to illustrate how mixing can impact the GOC and alter the stratification of the ocean and allow for testing of theoretical arguments and scalings. The general principle of stronger circulation with stronger mixing is illustrated in a comparison between Fig. 7a, b. In the latter, the increased diffusivity above 2000 m leads to a strengthening of the AMOC, stronger diabatic character and a deepening of the overall stratification. In an ocean model with an explicit diapycnal diffusivity set to almost zero, the bottom cell is particularly weak, as is the abyssal circulation in general[88].

Effects of circumpolar gateway
The thermocline scalings (Eq. (2)) fail when a portion of the domain is zonally unblocked, as in the Southern Ocean. In a channel, meridional heat transport is mediated by eddies rather than a western boundary current. The eddies are generated by baroclinic instability, requiring tilting isopycnals in the interior[89], and the resulting thermocline depth is much deeper than predicted by scaling. The same is true with a northern basin joined to a southern channel, assuming surface buoyancy fluxes produce denser waters in the south than in the north. Then the deep thermocline extends into the basin, all the way to the northern boundary, even in the presence of low mixing[90].

Simulations with realistic basins, prescribed turbulent diffusivity but no winds confirm the presence of a deep thermocline[84]. This is also observed by comparing the overturning circulation when the southern channel is open (Fig. 7a) or closed (Fig. 7c) in an idealized model configuration forced with the same applied wind. Stratification is deeper and the AMOC is stronger when the channel is opened. However, the bottom cell is stronger and extends over more of the water column if the channel is closed, indicating a possible competition between the two cells. Similar results have previously been found for both idealized[91] and realistic models[92] with blocked Southern Oceans. This is also consistent with the picture emerging of the early Eocene overturning with most modeling efforts and proxies indicating southern-dominated overturning[93,94] (see Section "Continental boundaries").
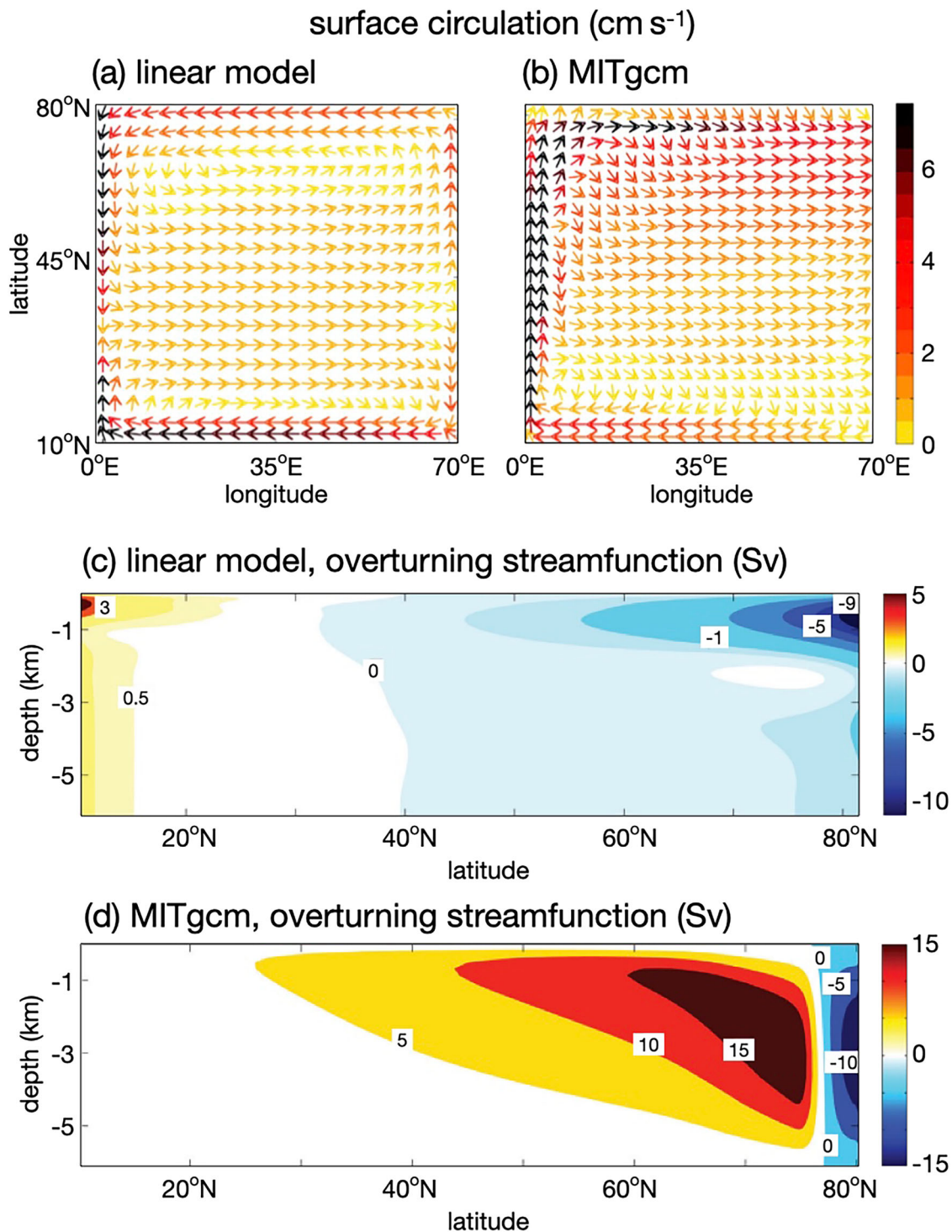
Adding wind pumping to the picture
Ekman transport drives a large portion of the volume transport near the ocean surface, and divergences and convergences in this transport control much of the circulation in the upper 700 m of the ocean basins. Wind pumping leads to the formation of wind-driven gyres in basins, with their associated intense western boundary currents. The presence of the Southern Ocean gateway greatly enhances the influence of Southern Hemisphere westerlies, allowing these winds to impact the stratification and overturning in the deep ocean. In this section we focus on the direct effect of wind pumping on the circulation.

Winds over the ocean basins
The wind-driven gyres result from Sverdrup transport in a zonally blocked geometry (as in a basin). The Sverdrup transport is returned in narrow western boundary currents. As noted earlier, *baroclinic* gyres are sometimes observed in numerical experiments forced by buoyancy only, but adding wind forcing greatly increases their strength and it also generates a barotropic transport[50,68,95]. The mean kinetic energy reservoir is more than an order of magnitude greater than in the barotropic case[51], as the Sverdrup transport produces surface-intensified horizontal velocities in a relatively shallow layer. Simultaneously, the strengthened western boundary current becomes more unstable, increasing eddy kinetic energy in the domain. This has a strong effect on air-sea buoyancy exchange[49,96,97], producing a nonlinear response of the circulation to wind changes.

Gyres are a three-dimensional circulation that projects onto the vertical, modulating the stratification of the upper ocean (Fig. 3c). Pumping (downwelling) in the subtropics and suction (upwelling) at the equator generates a characteristic W-shape in isopycnal depths above 400 m in the

surface circulation (cm s⁻¹)

(a) linear model

(b) MITgcm

(c) linear model, overturning streamfunction (Sv)

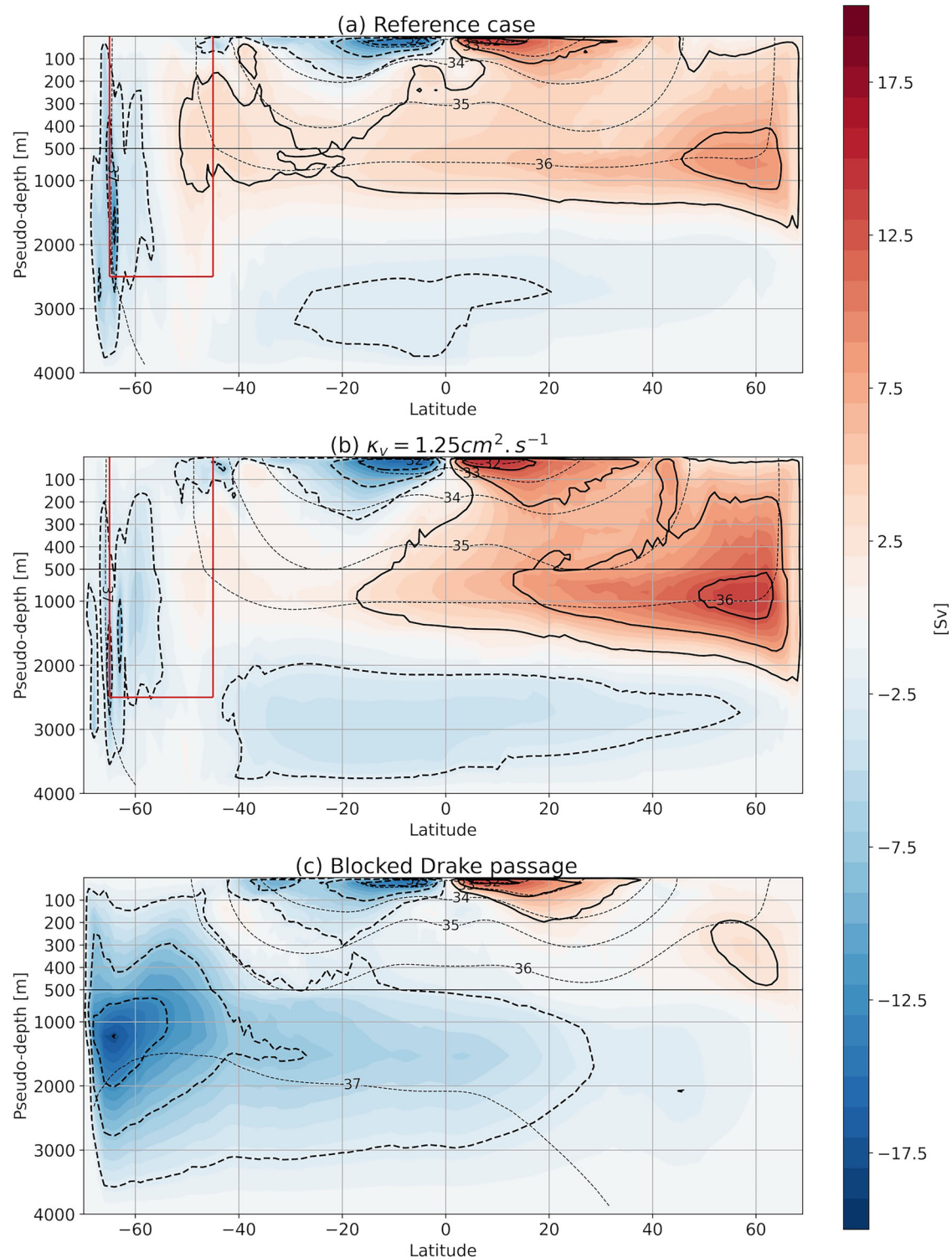### (d) MITgcm, overturning streamfunction (Sv)

Fig. 6 | Linear and nonlinear solutions for a buoyancy-driven circulation in a square basin. Surface circulation in **a** a linear, analytical model and **b** a nonlinear model solving the primitive equations using the MITgcm ocean model. The arrow colors indicate the flow speed. Corresponding overturning streamfunction in **c** the linear model and **d** the primitive equation simulation (red/positive is clockwise, blue/negative is anticlockwise). The analytical model is obtained by assuming a uniform (and typically constant) mean stratification. While such assumption is acceptable to represent low and mid-latitude dynamics, it precludes high-latitude convection, thus grossly misrepresenting the deep overturning cell. In contrast the nonlinear model has a parameterized representation of convection, drastically increasing vertical diffusivity in regions of static instability. As a result, it produces a realistic overturning cell, illustrating the central importance of convection in setting the deep overturning cell. Adapted from Gjermundsen and LaCasce[67].

meridional plane (Figs. 1a and 7). The effects of wind on thermocline depth have been explored in several studies that assume adiabatic circulation with prescribed density at the surface[98,99]. Extending these results to include diabatic effects, it was found that two thermoclines exist in the limit of small vertical diffusivity[95]. Closest to the surface is the ventilated thermocline, and

the depth of the wind-driven layer D_a is controlled by the scaling,

$$D_a \sim \left(\frac{W_E f L^2}{g \Delta b} \right)^{1/2}, \tag{3}$$

Fig. 7 | Residual meridional overturning streamfunction for different idealized configurations. Streamfunction computed in density coordinate, and then remapped in pseudo-depth coordinate[192], computed for three variants of the idealized DINO configuration[193] and run to near-equilibrium with the VEROS ocean model[194]. The contour interval is 5 Sv. Sigma-2 contours are superimposed in black dashed lines. **a** The reference 1° configuration, has an elongated 5000 km-wide basin with a 2500 m-deep re-entrant channel in the South (red box) mimicking the Southern Ocean. A zonal wind is applied at the surface, together with thermal and haline restoring to zonally-averaged climatological values. Eddies are parameterized using a GM-like scheme. A vertical diffusivity profile is prescribed, with 0.3 cm² s⁻¹ above 2000 m transitioning to 1.25 cm² s⁻¹ below 3000 m[195]. A typical overturning structure is obtained, with tropical cells in the upper thermocline, a deep AMOC-like cell and a bottom AABW-like cell originating from the southern edge. **b** The configuration is run with a constant 1.25 cm² s⁻¹ vertical diffusivity up to the surface, making the AMOC-like cell deeper and more intense but also more diabatic in the interior. Similarly, the tropical cell becomes deeper and stronger with increased diffusivity. **c** When the southern channel is blocked, the AMOC-like cell is nearly shut down while the bottom cell is now intensified due to a combination of wind pumping, southern convection and deep mixing. On the other hand, the tropical cells are nearly unchanged, illustrating their primarily wind-driven nature. The pycnocline depth is about 30% shallower than in the case of an open re-entrant channel.

where W_E is the downward Ekman pumping velocity and the other parameters are as in Eq. (2). The diffusive thermocline lies directly below this layer and its thickness follows Eq. (2). Though the direct effect of pumping on the pycnocline depth is sizable in a closed basin, the effect on the deep overturning strength is more limited[74] because the velocities that are directly driven by the wind forcing are confined primarily to the upper 300–500 m of the ocean.

Strong Ekman pumping in the equatorial Pacific and in the Atlantic sector of the Southern Ocean leads to large heat uptake in these regions[79]. As a result, more heating occurs close to the surface and less heating at depth (facilitated by mixing); this reduces the amount of energy put into the ocean circulation by heating at depth[51]. Though equatorial heating in the Pacific mainly affects subtropical cells, it is also thought to interact with the mid-depth cell in the tropical Pacific, where large ocean heat uptake contributes to the closure of the AMOC by transforming denser mid-depth waters into lighter surface waters[79,100]. These shallow overturning cells are obvious in the GOC when computed in temperature or density coordinates (see Fig. 1b), and contribute 40–50% of the peak Atlantic northward heat transport and nearly all of the peak meridional heat transport in the Pacific basin[101,102], providing a strong feedback on the surface buoyancy forcing.

Southern Ocean winds
In the Southern Ocean, eastward winds drive northward Ekman transport near the ocean surface[103]. The resulting Ekman pumping steepens the isopycnals, increasing the potential energy stored in the stratification. For a zonal mean eastward wind stress of 0.1–0.15 N m^{-2}, the Eulerian wind-driven overturning (the so-called Deacon cell, green dashed line in Fig. 3d) is about 40–50 Sv. The potential energy stored in the sloping isopycnals is released by baroclinic instability and the resulting eddies transport buoyancy and other tracers meridionally[104]. The net circulation consistent with air-sea buoyancy fluxes, the residual circulation[105,106], is of order 10 Sv, much smaller than the wind driven circulation[107]. Hence, the eddy-induced circulation of 30–40 Sv nearly cancels the wind-driven component (orange dashed line in Fig. 3d).

The residual circulation is a convenient framework to discuss the transport of buoyancy and other tracers and the influence of the Southern Ocean winds on the GOC north of Drake Passage (56–60°S). The adiabatic component of the residual circulation joins the surface of the North Atlantic with the surface of the Southern Ocean, crossing isopycnals only close to the ocean surface[108,109]. This component is represented by horizontal motions in Fig. 1b, but cannot be seen in Fig. 5a because by definition the adiabatic component of the circulation does not change density except at the surface. Diapycnal upwelling in the Atlantic, Indian and Pacific also contributes to the total AMOC transport[110,111], but the size of this contribution varies between models[41,112] and between different climate states[113].

The balance between pumping and eddies controls the slope of isopycnals in the Southern Ocean, which, in turn, controls the stratification in the Atlantic, Pacific, and Indian basins. A simplified budget of upper water volume leads to a cubic equation[114] for the depth of the pycnocline h,

$$\frac{Cg'}{\beta L_y^n}h^3 + \frac{K_e}{L_y^s}h^2 - \frac{\tau_0 L_x}{\rho f}h - \kappa_v A = 0, \qquad (4)$$

where the terms represent (1) deep water formation in the north, (2) the eddy transport in the Southern Ocean, (3) the volume transported by Southern Ocean Ekman transport, and (4) the transport across the pycnocline by vertical diffusion (see caption of Fig. 8 for notations). This model predicts that the stratification in the basins and the strength of North Atlantic deep water formation is strongly influenced by both the wind and the vertical diffusivity (Fig. 8b, e). If the Southern Ocean wind and eddies are set to zero, then the classical scaling of Eq. (2) is recovered. In the adiabatic limit ($\kappa_v = 0$), the depth of the AMOC is set by the depth of the isopycnal associated with NADW formation[108], and the depth of this isopycnal is controlled by the balance between wind and eddies in the Southern Ocean.

Various attempts at generalizing this simplified model have been proposed, in particular to account for the interaction between lower and upper overturning cells[109,115] or to differentiate the pycnocline depth in the Atlantic and Pacific basins and capture the dynamics of inter-basin exchanges between them[116]. It is believed that when the stratification is shallow (like during glacial periods[117]), dense AABW influences a wide range of depths and NADW cannot penetrate deep into the ocean. When the stratification is deeper (present day), AABW is more confined to the abyssal ocean, allowing the AMOC to penetrate to greater depth.

Eddy saturation and eddy compensation
In the above paradigm, increased wind steepens the isopycnal slope until the resulting eddy transport increases enough for equilibrium to be restored. Yet, in the early 2000s, multiple high-resolution numerical studies have shown that increasing wind directly drives more eddy transport without a substantial increase in isopycnal slope nor, through thermal wind balance, circumpolar volume transport—a process known as *eddy saturation*[73,118,119]. Recent work has shed new light on the physical mechanism underlying eddy saturation[120]. Zonal momentum input by the surface wind stress is transferred downward to the bottom through a combination of (1) eddy form stress and (2) residual overturning and associated Coriolis forces. The eddy form stress due to transient eddies is set by the eddy energy, and the source of this eddy energy must balance the bottom drag sink. In this regime, the circumpolar volume transport (excluding any contribution from bottom flow) is independent of the wind stress, but inversely proportional to the eddy energy damping time scale.

As a result of eddy saturation, if the wind is already strong, further increasing the wind may have a reduced impact on the residual overturning strength—a process known as *eddy compensation*. Nevertheless, in most eddy-resolving models, increasing the wind does tend to increase the AMOC strength to some extent because this eddy compensation is incomplete[119,121], and because changes in ocean surface wind affect the surface buoyancy forcing, which itself controls the strength of the overturning circulation[122]. The effects of partial and complete eddy compensation are illustrated in Fig. 8. In global simulations with parameterized eddy saturation, the isopycnal slope, depth of ocean stratification, and GOC are all found to increase with surface wind stress, albeit at a reduced rate[123]. The residual overturning is here sensitive to the time scale over which the parameterized eddy energy is dissipated, highlighting the importance of eddy dissipation processes in the dynamics of the GOC.

Complications due to thermohaline forcing and the nonlinear equation of state
An aspect that can significantly complicate the picture is the competition between heat and freshwater fluxes in determining the buoyancy forcing. Under mixed surface boundary conditions, i.e., when imposing simultaneously a surface thermal relaxation and freshwater fluxes, multiple stable states can exist[77,124,125]. It has been hypothesized that this may explain rapid variability of the AMOC and associated abrupt climate changes during the last glacial cycle although a definite proof is still lacking[126].

Under the on-going anthropogenically-driven climate change, freshwater input in the high latitudes is expected to increase which could have a similar destabilizing effect on the AMOC. In fully coupled simulations, freshwater input in so-called "hosing experiments" can weaken the overturning[3]. Though it is often stated that freshwater impacts the overturning by hindering convection, the impact is actually rather on the meridional buoyancy gradient itself[53]. It is also worth noting that in coupled simulations with increased atmospheric CO_2, freshwater input occurs because of melting sea ice and increased run-off[127], both of which result from a warming atmosphere. This is not the case in externally hosed experiments[128], meaning the climate response can be very different (e.g., wide-spreading cooling at northern latitudes not seen in coupled simulations).

The nonlinearity of the equation of state has also important effects on the global water-mass distribution and global overturning
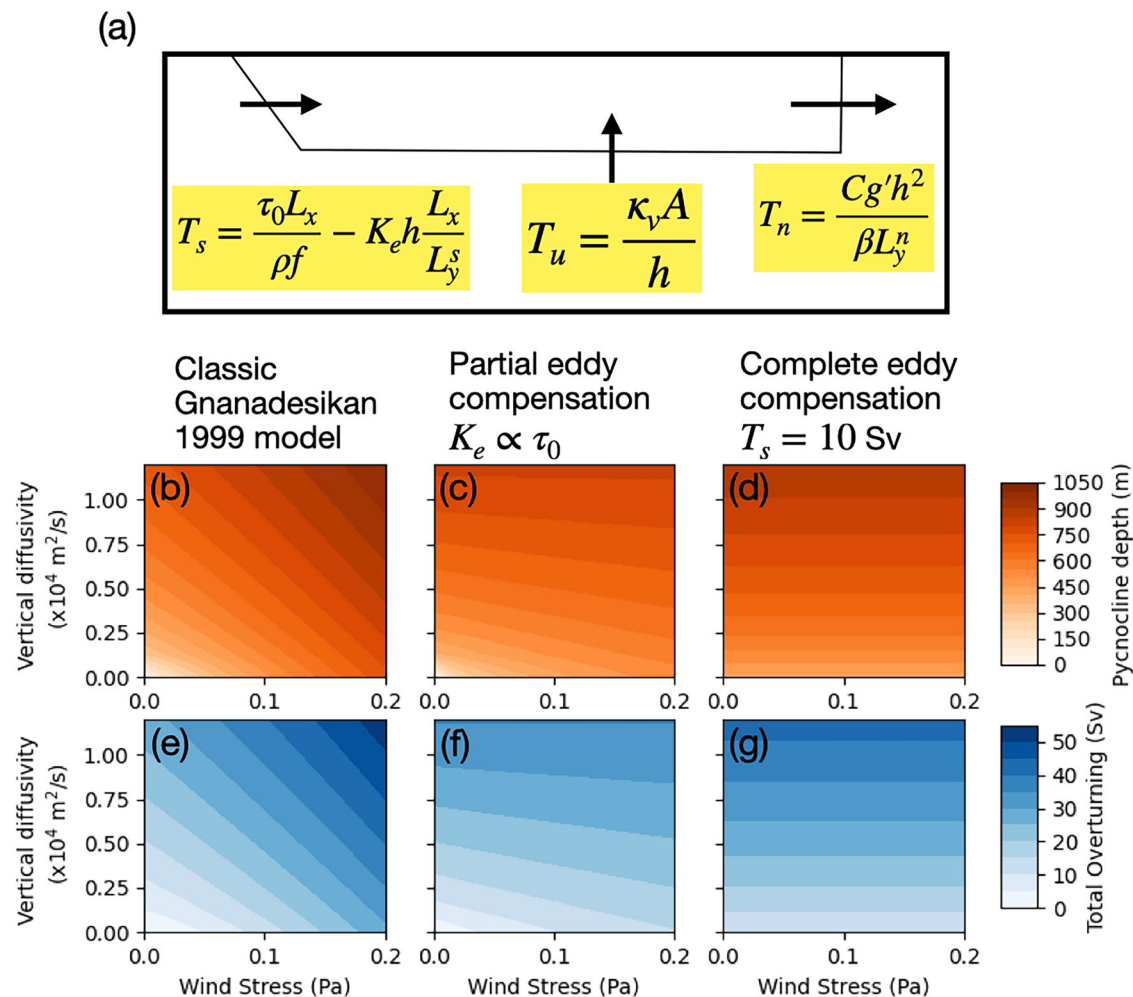
Fig. 8 | Conceptual model of the GOC and associated scalings. a Conceptual model created by Gnanadesikan[114] which uses simple scalings to model the volume transport across the pycnocline in the North Atlantic, in the tropics and subtropics and in the Southern Ocean. Important parameters include g' the reduced gravity, proportional to density difference between the two layers, K_e the thickness diffusivity associated with the eddy closure, τ_0 the Southern Ocean wind stress, f and β the Coriolis and beta parameters at mid-latitude, and κ_v the vertical diffusivity. Geometric parameters L_y^s and L_y^n are the meridional widths of the channel and North Atlantic, respectively, and L_x is the zonal width of the Atlantic basin. C is a constant factor representing the geometry of the North Atlantic. The scaling thus obtained is used to illustrate some basic sensitivities for, **b** the pycnocline depth; **e** the associated overturning transport. Recent modeling studies suggest that increasing the wind stress leads to an increase in the thickness diffusivity due to increased eddy generation[73]. This produces so-called eddy compensation, illustrated in the center panels **c** and **f** by setting K_e proportional to τ_0. In the bottom right panels **d** and **g**, T_s is fixed at 10 Sv, synonymous with complete eddy compensation.

circulation[129]. It influences the deep water mass layering through thermobaricity[130] and subduction rates in the Southern Ocean through cabbelling[130,131]. This affects also the distribution of surface buoyancy fluxes, favoring dominance of freshwater over heat fluxes in high latitudes[132]. This happens primarily because the thermal expansion coefficient increases with increasing temperature, making cold water very weakly sensitive to heat fluxes and temperature stratification. This nonlinearity provides a potentially powerful feedback mechanism between the climate and the ocean stratification. In cold climates, salinity becomes a stronger stratifying agent and the ocean becomes more stratified and less well ventilated[129,133,134]. This might explain the transition to the Pleistocene cycle of ice ages, 2.7 million years ago[135].
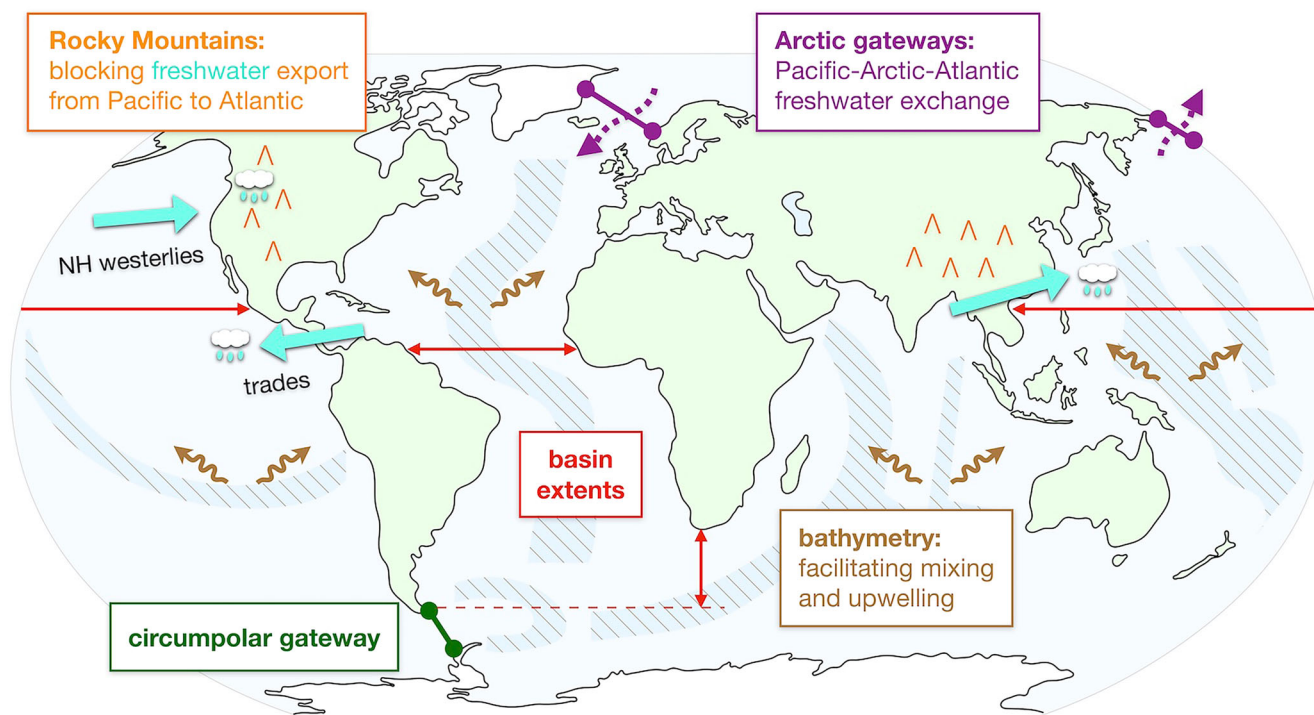
Geographic controls
On geological timescales (>1 million years), geography itself becomes a dominant control of the ocean circulation. At these long time scales, the circulation can be considered in an equilibrium state set by the ocean-land geometry and the surface forcing. Geography controls the circulation in three main ways: through ocean basin geometry, modulation of mixing and land orography (Fig. 9).

Continental boundaries
In the present-day, the most pronounced geometric characteristics are two large inter-hemispheric ocean basins, separated by continents that form meridional boundaries between them. Importantly, there is a circumpolar channel in the narrow latitude band of Drake Passage that formed in the late Eocene, about 40 million years ago, as South America and Australia gradually separated from Antarctica[136]. The formation of this zonally re-entrant channel was key to the establishment of the modern meridionally asymmetric overturning[137].

Today, Northern Hemisphere deep water formation occurs preferentially in the Atlantic, though that has not always been the case. A growing body of evidence points to a non-existent or weak AMOC in the early Eocene, which over the next 50 million years evolved to the strong inter-hemispheric circulation it is today[138]. In contrast, a stronger Pacific Meridional Overturning Circulation (PMOC) in the early Eocene weakened over time, and in the last 15 million years has become more of an occasional feature of the GOC[139,140]. These contrasting trends were probably linked to both geographic changes and the overall cooling climate. An early constraint on Atlantic deepwater formation was the Atlantic's connection with a very fresh Arctic, which

Fig. 9 | Schematic of geographic controls important to the GOC. Two large, inter-hemispheric ocean basins of different widths are separated by continents of different length (basin extents indicated by red arrows). In the Southern Hemisphere, the open Drake Passage (green gateway indicator) allows for circumpolar flow and facilitates a north-south asymmetry in the overturning. In the Northern Hemisphere, freshwater is exchanged between the North Pacific, fresh Arctic, and North Atlantic, through the Arctic straits. Atmospheric freshwater transport (cyan arrows) is affected by orographic features such as the Rocky Mountains, which blocks freshwater transport from the Pacific to the Atlantic, thus increasing the salinity of the Atlantic at the expense of the Pacific[167]. In contrast, freshwater transport from the Atlantic is carried unhindered to the Pacific by the Trade winds[196]. The elevated Tibetan Plateau strengthens the East Asian monsoon circulation and the related freshwater supply to the North Pacific[197], and can therefore arrest a PMOC in favor of an AMOC[198]. Bathymetry (brown box) facilitates mixing and upwelling. Because of bottom drag and seafloor roughness, submarine topography (shaded and dashed patches) catalyzes kinetic energy dissipation and mixing (brown wiggly arrows)[199,200], thus setting the overall circulation balance and shaping the distribution of mechanical mixing. The distribution and global magnitude of tidal dissipation are sensitive to the arrangement of continental shelves and slopes as well as ridges, seamounts and abyssal hills[201]. In addition, the depth distribution of the seafloor controls the rate of upwelling across isopycnals[87].

reached salinities of order 20–25 g/kg in the early to middle Eocene[141]. Recent studies have suggested that, leading up to the Eocene-Oligocene Transition (~34 Ma) when Antarctica became glaciated, the temporary restriction or closure of Arctic-Atlantic gateways led to a stepwise increase in North Atlantic salinity and thus triggered the first deepwater formation in the Atlantic[142].

During the Miocene (23 to 5 Ma), as polar gateways continued to widen, the tropical seaways narrowed, shoaled and eventually closed off freshwater exchange between the Indo-Pacific and Atlantic basins at low latitudes. The first to close off was the Tethys seaway around 14–22 Ma[143] followed around 3–6 Ma by the Central American seaway[144]. The exact impact of these tropical gateway closures on the AMOC remains unclear; they have alternatively been suggested as crucial[145,146] or inconsequential[143,147] for the development of the AMOC.

A more recent geographical development is the opening of the Bering Strait, which created a northern passage between the Pacific and the Atlantic near 5.5 Ma[148]. This probably enhanced freshwater transport from the Arctic to the Atlantic and reduced the AMOC. This link between the GOC and Bering Strait was evident in recent climate model simulations of the mid Pliocene (~3 Ma), which had a closed Bering Strait and consistently featured a stronger AMOC than in pre-industrial simulations with the same models[149]. On more recent time scales, the strait is generally thought to have a stabilizing effect on the AMOC[150], in that it allows for the reversal of the Pacific-Atlantic freshwater transport when the AMOC is sufficiently weakened[151,152], although some studies conclude otherwise[153].

A continuous, large-scale paleogeographic change over the last ~50 million years has been the widening of the Atlantic basin at the expense of a narrowing Pacific basin. Several idealized modeling studies have suggested that the narrow width of the Atlantic makes it the preferred basin for downwelling, with explanations focusing on both wind and freshwater forcings in the basins[154,155]. In contrast, other studies found that a widening of the Atlantic leads to an increase in AMOC, and that the increase is sensitive to the meridional structure of, in particular, the American continent[156]. The paleorecord supports the latter result, with an increasing dominance in the AMOC as the Atlantic widened[138]. Finally, the lesser southward reach of the African continent (33°S) relative to the American continent (55°S), via its impact on Agulhas salt leakage, has been suggested as another reason for preferential sinking in the Atlantic[157].

Bathymetry
Submarine topography is a critical ingredient controlling the GOC through catalysis of dissipation and mixing, setting the overall circulation balance and shaping the distribution of mechanical mixing. Friction at the bottom boundary plays a fundamental role in breaking geostrophy and allowing downslope flows that make up the downwelling limbs of the GOC. The detailed shape of ocean basins is particularly influential for tidal dissipation (Fig. 9). Given that tides are the leading contributor to mixing in the ocean interior[34], tectonics and changes in sea level can have pronounced impacts on the GOC via tidal mixing[158,159]. Sills and straits connecting deep sub-basins also play an outsize role in shaping abyssal circulation and stratification, because they host swift flows and extreme turbulent mixing rates[160,161].

Because seafloor-catalyzed turbulence is bottom-enhanced, and because of geothermal heating, buoyancy gain in the deep ocean is largely
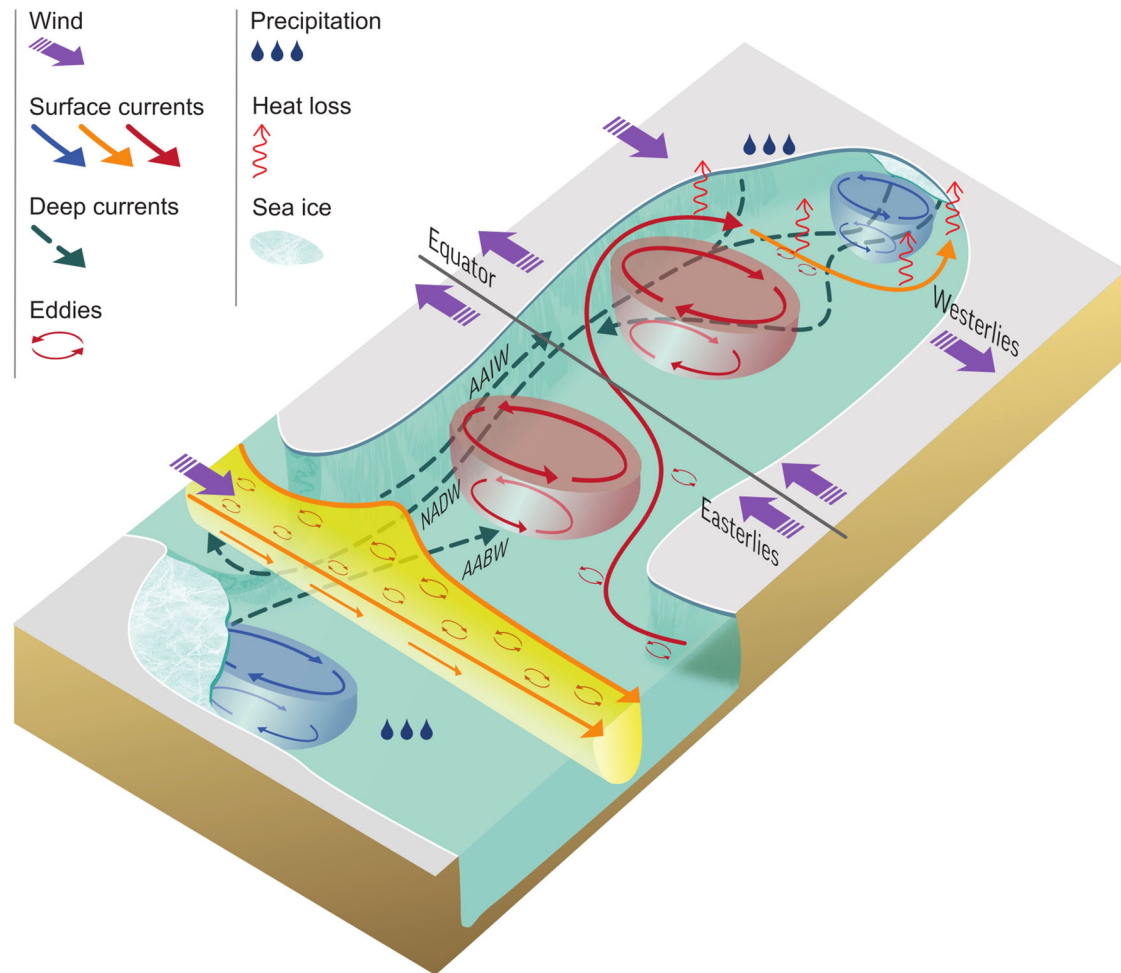
Fig. 10 | Schematic of forcings important to the GOC in the Atlantic sector and how they generate different flow patterns that collectively generate the meridional overturning flow. Changes in sea ice extent, wind strength, cooling and precipitation all have the potential to deeply impact the GOC. The wind strength modifies the pumping and modulates gyres and Antarctic Circumpolar Current (ACC) transports. Cooling and sea ice production activate deep convection in the high latitudes, while precipitation can hinder it. Inter-hemispheric flow of water masses depends on a three-way balance between deep water formation, northward Ekman transport across the ACC and interior mixing. Eddy compensation partially reduces the impact of southern winds on the residual overturning. Each major water mass formation site is associated with a deep water mass: Antarctic shelves for Antarctic Bottom Water (AABW), subpolar North Atlantic seas for North Atlantic Deep Water (NADW) and the northern edge of the ACC for Antarctic Intermediate Water (AAIW). The resulting overturning transport varies at all timescales, ranging from interannual to multi-centennial, making it a great challenge to adequately observe and to correctly reproduce in numerical models.

confined to a thin bottom ocean layer[162] and it plays a key role in controlling the circulation of AABW[35] and possibly NADW as well[41]. In the current ocean geometry, the seafloor is relatively abundant deeper than 2.5 km, and relatively scarce between 0.5 and 2.5 km depth. As a result, the abyssal overturning is confined to depths greater than 2.5 km, creating a relatively isolated and carbon-rich Pacific shadow zone between the wind-driven upper ocean and the turbulent abyss[87,163].

A similar argument can be made for different (past) geometries. Although the depth distribution of the seafloor in the deep past is poorly known, it is likely that mid-depth oceanic shadow zones have existed and varied in volume with plate tectonics (and shifting oceanic deepwater formation sites). Such linkages between ocean circulation and seafloor distribution provide a plausible climate-geology coupling on million-year time scales, potentially complementary to the silicate weathering and mountain creation control on atmospheric CO_2[164,165].

Orography
The topography of the land also exerts a first-order impact on the GOC, both through its control of atmospheric freshwater transport and by inducing the observed interhemispheric asymmetry of midlatitude zonal wind stress, with much stronger westerlies in the Southern Hemisphere[166]. In general, present orography favors an AMOC at the expense of a PMOC, as the removal of global orography tends to switch deep overturning to the Pacific[167,168]. The Rocky Mountains, the Tibetan Plateau, and the Panama Isthmus are orographic features that influence atmospheric freshwater transports in a way that redistributes freshwater from the Atlantic and Indian to the Pacific (Fig. 9). Here, the Rocky Mountains are considered to be of major importance, but the Rocky Mountains uplifted ~80 Ma and reached their current height at ~40 Ma, before the onset of the modern day AMOC, suggesting it is merely a contributing factor to the Atlantic dominance of northern overturning.

Conclusion
The overarching theme of this review is the great complexity of the global overturning circulation (GOC), as illustrated for the Atlantic sector in Fig. 10. The GOC is not governed by a single dominant "driver" but rather emerges from the interplay of multiple processes that vary in space, time, and energetic contribution. We noted that the term *driver* can lead to confusion; instead, it's more accurate to consider power sources, controls, and forcings separately. This is why we focused here on the controls of the GOC.

In summary (see Fig. 3):

- Differential buoyancy fluxes at the surface, even in the absence of winds or mixing, can produce a global overturning circulation with very shallow stratification (horizontal convection regime).
- Mechanical mixing powered by wind and tides strongly enhances the overturning produced by surface buoyancy fluxes, and is central to the existence of a realistic stratification.
- Wind pumping generates shallow tropical cells and intense western boundary currents, deepening the stratification in the subtropics.
- Westerly winds over the circumpolar Southern Ocean create an upwelling hotspot that increases both the depth and the strength of the GOC.

These different controls do not act in isolation (Fig. 2): they interact strongly with one another and are also constrained by the geometry of the physical boundary condition. Mechanical mixing enhances buoyancy-driven convection by deepening the thermocline, which in turn modulates the overturning response to wind forcing. The geographic coincidence of a circumpolar channel with strong Southern Hemisphere westerlies is particularly effective at driving a vigorous inter-hemispheric overturning circulation and at shaping the global stratification. This has major implications for the GOC of the past, as this key coincidence has not been present during much of Earth's history.

In addition to external forcings, internal processes—particularly those related to energy conversion and dissipation—play a fundamental role in shaping the GOC. Eddies generated by baroclinic instability, especially in the Southern Ocean, influence both isopycnal and diapycnal transport. However, key questions remain about the fate of this eddy energy: How is it dissipated, and what effect does this dissipation have on the large-scale circulation? Current eddy parameterizations such as Gent-McWilliams (GM) eliminate large amounts of eddy energy through idealized diffusion, but the real ocean may redirect this energy through pathways such as convection or turbulence. These uncertainties highlight the importance of better understanding how energy dissipation shape the structure and variability of the GOC.

Future challenges

Climate models are essential tools for exploring the GOC, but they face persistent challenges. Models continue to exhibit large disagreements in how they simulate the GOC, especially in response to changing wind, tidal, and buoyancy forcing. Convection, overflows, and internal mixing processes remain poorly represented in climate models. Even increasing the model resolution does not guarantee improved realism[169,170]—despite prohibitive computational costs. As a result, predictions for overturning strength in both modern and paleo-climate contexts vary widely across models[171,172] leading to large uncertainties in projections of future heat and carbon transport[112]. Of particular interest is the fate of the AMOC under future climate. The AMOC is predicted to weaken, but not collapse, according to most climate models[173]. While the range of weakening by the end of the 21st century is very large, models predicting larger AMOC weakening are the ones associated with larger biases in ocean stratification[174]. These discrepancies raise serious concerns about whether our current models can be trusted to predict the evolution of the GOC in the next century and beyond.

Furthermore, progress is limited by the metrics we use to evaluate the GOC. Overemphasis on the maximum value of the AMOC streamfunction may lead to misleading interpretations. The streamfunction in depth-latitude space is dominated by stationary eddies, while density-latitude space blurs the connection to surface air-sea fluxes (Fig. 1). The streamfunction in depth-density space captures the diapycnal component of the flow, and can be readily connected to energy conversion (Fig. 5), however it remains difficult to interpret, is not frequently applied, and has limited information about the geometry of the circulation. Streamfunctions provide information about the integrated flow, but are not straightforward to compare to modern observations or proxies of past overturning[175]. In this regard, other diagnostics of deep ocean overturning, such as the ventilation

age of the water, the strength of deep Western Boundary currents, the depth of convection, and tracers of water masses may be more useful. These may also be more relevant for identifying features of the overturning that impact its role in the carbon cycle. Understanding how these different diagnostics relate to each other and what energy constraints shape their structure is an important area for future research.

The configuration and sensitivity of the GOC have likely changed substantially under different climate and geographic conditions in the past, and will continue to evolve in the future. Changes in convection, mixing, and wind-driven processes all contribute to long-term variability. Understanding these changes is critical not only for climate projections[176,177], but also for carbon storage in the ocean and atmosphere[178–180], and even for assessing habitability of ocean-bearing exoplanets[181].

In the long term, the ability to sustain global observations—from both satellites[182] and in situ platforms[183]—will be critical to better constraining and validating models[184]. Coupled with new tools, better diagnostics, and a deeper understanding of the physical and energetic constraints on circulation, these advances will help us address one of the most pressing challenges in oceanography: understanding and predicting the variability and future evolution of the GOC.

Data availability

References

1. Cessi, P. The global overturning circulation. *Annu. Rev. Mar. Sci.* **11**, 249–270 (2019).
2. Broecker, W. S. Unpleasant surprises in the greenhouse? *Nature* **328**, 123–126 (1987).
3. Weijer, W. et al. Stability of the Atlantic meridional overturning circulation: a review and synthesis. *J. Geophys. Res. Oceans* **124**, 5336–5375 (2019).
4. Li, Q., England, M. H., Hogg, A. M., Rintoul, S. R. & Morrison, A. K. Abyssal ocean overturning slowdown and warming driven by Antarctic meltwater. *Nature* **615**, 841–847 (2023).
5. Jackson, L. C. et al. Global and European climate impacts of a slowdown of the AMOC in a high resolution GCM. *Clim. Dyn.* **45**, 3299–3316 (2015).
6. Swart, N. C., Gille, S. T., Fyfe, J. C. & Gillett, N. P. Recent Southern Ocean warming and freshening driven by greenhouse gas emissions and ozone depletion. *Nat. Geosci.* **11**, 836 (2018).
7. Bonan, D. B., Thompson, A. F., Newsom, E. R., Sun, S. & Rugenstein, M. Transient and equilibrium responses of the Atlantic overturning circulation to warming in coupled climate models: the role of temperature and salinity. *J. Clim.* **35**, 5173–5193 (2022).
8. Gray, W. R. et al. Poleward shift in the Southern Hemisphere westerly winds synchronous with the deglacial rise in CO2. *Paleoceanogr. Paleoclimatol.* **38**, e2023PA004666 (2023).
9. Liu, Y., Moore, J. K., Primeau, F. & Wang, W. L. Reduced CO2 uptake and growing nutrient sequestration from slowing overturning circulation. *Nat. Clim. Change* **13**, 83–90 (2023).
10. Broecker, W. S. The great ocean conveyor. *Oceanography* **4**, 79–89 (2015).
11. Lozier, M. S. Deconstructing the conveyor belt. *Science* **328**, 1507–1511 (2010).

12. Marshall, J. & Speer, K. Closure of the meridional overturning circulation through Southern Ocean upwelling. *Nat. Geosci.* **5**, 171–180 (2012).

13. Kuhlbrodt, T. On Sandström's inferences from his tank experiments: a hundred years later. *Tellus A Dyn. Meteorol. Oceanogr.* **60**, 819–836 (2008).

14. Munk, W. & Wunsch, C. Abyssal recipes II: energetics of tidal and wind mixing. *Deep Sea Res. Part I Oceanogr. Res. Pap.* **45**, 1977–2010 (1998).

15. Toggweiler, J. R. & Samuels, B. On the ocean's large-scale circulation near the limit of no vertical mixing. *J. Phys. Oceanogr.* **28**, 1832–1852 (1998).

16. Paparella, F. & Young, W. R. Horizontal convection is non-turbulent. *J. Fluid Mech.* **466**, 205–214 (2002).

17. Wunsch, C. & Ferrari, R. Vertical mixing, energy, and the general circulation of the oceans. *Annu. Rev. Fluid Mech.* **36**, 281–314 (2004).

18. Kuhlbrodt, T. et al. On the driving processes of the Atlantic meridional overturning circulation. *Rev. Geophys.* **45**, RG2001 (2007).

19. Burchard, H. et al. Linking ocean mixing and overturning circulation. *Bull. Am. Meteorol. Soc.* **1**, https://doi.org/10.1175/BAMS-D-24-0082.1 (2024).

20. Vreugdenhil, C. A. & Gayen, B. Ocean convection. *Fluids* **6**, 360 (2021).

21. Wunsch, C. Is the ocean speeding up? Ocean surface energy trends. *J. Phys. Oceanogr.* **50**, 3205–3217 (2020).

22. Wang, W. & Huang, R. X. Wind energy input to the surface waves. *J. Phys. Oceanogr.* **34**, 1276–1280 (2004).

23. Rimac, A., von Storch, J.-S. & Eden, C. The total energy flux leaving the ocean's mixed layer. *J. Phys. Oceanogr.* **46**, 1885–1900 (2016).

24. Wang, W. & Huang, R. X. Wind energy input to the Ekman layer. *J. Phys. Oceanogr.* **34**, 1267–1275 (2004).

25. Zhai, X., Greatbatch, R. J., Eden, C. & Hibiya, T. On the loss of wind-induced near-inertial energy to turbulent mixing in the upper ocean. *J. Phys. Oceanogr.* **39**, 3040–3045 (2009).

26. Gaspar, P., Grégoris, Y. & Lefevre, J.-M. A simple eddy kinetic energy model for simulations of the oceanic vertical mixing: tests at station Papa and long-term upper ocean study site. *J. Geophys. Res. Oceans* **95**, 16179–16193 (1990).

27. Huang, R. X. & Wang, W. Gravitational potential energy sinks in the oceans. in *Near-Boundary Processes and Their Parameterization, Proceedings, 'Aha Huliko'a Hawaii Winter Workshop* (eds Muller, P. & Henderson, D.) 239–247 (University of Hawaii, 2003).

28. Whalen, C. B. et al. Internal wave-driven mixing: governing processes and consequences for climate. *Nat. Rev. Earth Environ.* **1**, 606–621 (2020).

29. Kunze, E. Internal-wave-driven mixing: global geography and budgets. *J. Phys. Oceanogr.* **47**, 1325–1345 (2017).

30. Egbert, G. D. & Ray, R. D. Significant dissipation of tidal energy in the deep ocean inferred from satellite altimeter data. *Nature* **405**, 775–778 (2000).

31. Egbert, G. D. & Ray, R. D. Estimates of M2 tidal energy dissipation from TOPEX/Poseidon altimeter data. *J. Geophys. Res. Oceans* **106**, 22475–22502 (2001).

32. Geoffroy, G., Kelly, S. M. & Nycander, J. Tidal conversion into vertical normal modes by continental margins. *Geophys. Res. Lett.* **52**, e2024GL112865 (2025).

33. Webb, D. J. & Suginohara, N. Oceanography. vertical mixing in the ocean. *Nature* **409**, https://doi.org/10.1038/35051171 (2001).

34. de Lavergne, C. et al. A parameterization of local and remote tidal mixing. *J. Adv. Model. Earth Syst.* **12**, e2020MS002065 (2020).

35. de Lavergne, C., Groeskamp, S., Zika, J. & Johnson, H. L. Chapter 3—the role of mixing in the large-scale ocean circulation. in *Ocean Mixing* (eds Meredith, M. & Naveira Garabato, A.) 35–63 (Elsevier, 2022).

36. Roquet, F., Wunsch, C. & Madec, G. On the patterns of wind-power input to the ocean circulation. *J. Phys. Oceanogr.* **41**, 2328 – 2342 (2011).

37. Storch, J.-Sv et al. An estimate of the Lorenz energy cycle for the world ocean based on the STORM/NCEP simulation. *J. Phys. Oceanogr.* **42**, 2185–2205 (2012).

38. Gent, P. R. & McWilliams, J. C. Isopycnic mixing in ocean circulation models. *J. Phys. Oceanogr.* **20**, 150–155 (1990).

39. Nycander, J., Nilsson, J., Döös, K. & Broström, G. Thermodynamic analysis of ocean circulation. *J. Phys. Oceanogr.* **37**, 2038–2052 (2007).

40. Forget, G. et al. ECCO version 4: an integrated framework for non-linear inverse modeling and global ocean state estimation. *Geosci. Model Dev.* **8**, 3071–3104 (2015).

41. Cimoli, L. et al. Significance of diapycnal mixing within the Atlantic meridional overturning circulation. *AGU Adv.* **4**, e2022AV000800 (2023).

42. Döös, K. & Webb, D. J. The Deacon cell and the other meridional cells of the southern ocean. *J. Phys. Oceanogr.* **24**, 429–442 (2011).

43. Gayen, B. & Griffiths, R. W. Rotating horizontal convection. *Annu. Rev. Fluid Mech.* **54**, null (2022).

44. Nycander, J. Horizontal convection with a non-linear equation of state: generalization of a theorem of Paparella and Young. *Tellus A Dyn. Meteorol. Oceanogr.* **62**, 134–137 (2010).

45. McIntyre, M. E. On spontaneous imbalance and ocean turbulence: generalizations of the paparella-young epsilon theorem. in *Turbulence in the Atmosphere and Oceans* (ed. Dritschel D.) 3–15 (Springer, 2010).

46. Scotti, A. & White, B. Is horizontal convection really "non-turbulent?". *Geophys. Res. Lett.* **38**, https://doi.org/10.1029/2011GL049701 (2011).

47. Hughes, G. O., Hogg, A. M. C. & Griffiths, R. W. Available potential energy and irreversible mixing in the meridional overturning circulation. *J. Phys. Oceanogr.* **39**, 3130–3146 (2009).

48. Colin de Verdière, A. Buoyancy driven planetary flows. *J. Mar. Res.* **46**, https://elischolar.library.yale.edu/journal_of_marine_research/1887 (1988).

49. Cronin, M. F. et al. Air-sea fluxes with a focus on heat and momentum. *Front. Mar. Sci.* **6**, 430 (2019).

50. Colin de Verdière, A. On the interaction of wind and buoyancy driven gyres. *J. Mar. Res.* **47**, 595–633 (1989).

51. Roquet, F. Dynamical potential energy: a new approach to ocean energetics. *J. Phys. Oceanogr.* **43**, 457–476 (2013).

52. Yeager, S. & Danabasoglu, G. The origins of late-twentieth-century variations in the large-scale north atlantic circulation. *J. Clim.* **27**, 3222–3247 (2014).

53. Madan, G., Gjermundsen, A., Iversen, S. C. & LaCasce, J. H. The weakening AMOC under extreme climate change. *Clim. Dyn.* **62**, 1291–1309 (2024).

54. Couldrey, M. P. et al. Greenhouse-gas forced changes in the Atlantic meridional overturning circulation and related worldwide sea-level change. *Clim. Dyn.* **60**, 2003 – 2039 (2023).

55. Stommel, H., Arons, A. & Faller, A. Some examples of stationary planetary flow patterns in bounded basins. *Tellus* **10**, 179–187 (1958).

56. Swallow, J. C. & Worthington, L. V. Measurements of deep currents in the Western North Atlantic. *Nature* **179**, 1183–1184 (1957).

57. Robinson, A. & Stommel, H. The oceanic thermocline and the associated thermohaline circulation. *Tellus* **11**, 295–308 (1959).

58. Welander, P. An advective model of the ocean thermocline. *Tellus* **11**, 309–318 (1959).

59. Robinson, A. & Welander, P. Thermal circulation on a rotating sphere; with application to the oceanic thermocline. *J. Mar. Res.* **21**, https://elischolar.library.yale.edu/journal_of_marine_research/991 (1963).

60. Bryan, K. & Cox, M. D. A numerical investigation of the oceanic general circulation. *Tellus* **19**, 54–80 (1967).

61. Welander, P. A discussion on ocean currents and their dynamics—the thermocline problem. *Philos. Trans. R. Soc. Lond. Ser. A Math. Phys. Sci.* **270**, 415–421 (1971).

62. Johnson, H. L., Cessi, P., Marshall, D. P., Schloesser, F. & Spall, M. A. Recent contributions of theory to our understanding of the Atlantic meridional overturning circulation. *J. Geophys. Res. Oceans* **124**, 5376–5399 (2019).

63. Munk, W. H. Abyssal recipes. *Deep Sea Res. Oceanogr. Abstr.* **13**, 707–730 (1966).

64. Pedlosky, J. Linear theory of the circulation of a stratified ocean. *J. Fluid Mech.* **35**, 185–205 (1969).

65. Salmon, R. A simplified linear ocean circulation theory. *J. Mar. Res.* **44**, https://elischolar.library.yale.edu/journal_of_marine_research/1832 (1986).

66. LaCasce, J. Diffusivity and viscosity dependence in the linear thermocline. *J. Mar. Res.* **62**, https://elischolar.library.yale.edu/journal_of_marine_research/61 (2004).

67. Gjermundsen, A. & LaCasce, J. H. Comparing the linear and nonlinear buoyancy-driven circulation. *Tellus A Dyn. Meteorol. Oceanogr.* **69**, 1299282 (2017).

68. Hogg, A. M. & Gayen, B. Ocean gyres driven by surface buoyancy forcing. *Geophys. Res. Lett.* **47**, e2020GL088539 (2020).

69. Spall, M. A. & Pickart, R. S. Where does dense water sink? A subpolar gyre example. *J. Phys. Oceanogr.* **31**, 810–826 (2001).

70. Brüggemann, N. & Katsman, C. A. Dynamics of downwelling in an eddying marginal sea: contrasting the eulerian and the isopycnal perspective. *J. Phys. Oceanogr.* **49**, 3017–3035 (2019).

71. Marotzke, J. & Scott, J. R. Convective mixing and the thermohaline circulation. *J. Phys. Oceanogr.* **29**, 2962–2970 (1999).

72. Bryan, F. Parameter sensitivity of primitive equation ocean general circulation models. *J. Phys. Oceanogr.* **17**, 970–985 (1987).

73. Munday, D. R., Johnson, H. L. & Marshall, D. P. Eddy saturation of equilibrated circumpolar currents. *J. Phys. Oceanogr.* **43**, 507–532 (2013).

74. Rosenthal, B. & Roquet, F. The center of mass of the ocean as an index of the general stratification and its relation to the overturning circulation. *J. Phys. Oceanogr.* **55**, 277–291 (2025).

75. Nadeau, L.-P. & Jansen, M. F. Overturning circulation pathways in a two-basin ocean model. *J. Phys. Oceanogr.* **50**, 2105–2122 (2020).

76. Marotzke, J. Boundary mixing and the dynamics of three-dimensional thermohaline circulations. *J. Phys. Oceanogr.* **27**, 1713–1728 (1997).

77. Zhang, J., Schmitt, R. W. & Huang, R. X. The relative influence of diapycnal mixing and hydrologic forcing on the stability of the thermohaline circulation. *J. Phys. Oceanogr.* **29**, 1096–1108 (1999).

78. Park, Y.-G. & Bryan, K. Comparison of thermally driven circulations from a depth-coordinate model and an isopycnal-layer model. Part I: scaling-law sensitivity to vertical diffusivity. *J. Phys. Oceanogr.* **30**, 590–605 (2000).

79. Bell, M. J., Nurser, A. J. G. & Storkey, D. Interpretation of net surface heat fluxes and meridional overturning circulations in global coupled HadGEM3 climate simulations. *J. Phys. Oceanogr.* **53**, 1555–1575 (2023).

80. Huang, R. X. Mixing and energetics of the oceanic thermohaline circulation. *J. Phys. Oceanogr.* **29**, 727–746 (1999).

81. Nilsson, J. & Walin, G. Freshwater forcing as a booster of thermohaline circulation. *Tellus A* **53**, 629–641 (2001).

82. Hieronymus, M., Nycander, J., Nilsson, J., Döös, K. & Hallberg, R. Oceanic overturning and heat transport: the role of background diffusivity. *J. Cim.* **32**, 701–716 (2019).

83. Melet, A., Hallberg, R., Legg, S. & Polzin, K. Sensitivity of the ocean state to the vertical distribution of internal-tide-driven mixing. *J. Phys. Oceanogr.* **43**, 602–615 (2013).

84. Gjermundsen, A., LaCasce, J. H. & Denstad, L. The thermally driven ocean circulation with realistic bathymetry. *J. Phys. Oceanogr.* **48**, 647–665 (2018).

85. Spall, M. A. An overlooked component of the meridional overturning circulation. *J. Phys. Oceanogr.* **54**, 1921–1932 (2024).

86. Ferrari, R., Mashayek, A., McDougall, T. J., Nikurashin, M. & Campin, J.-M. Turning ocean mixing upside down. *J. Phys. Oceanogr.* **46**, 2239–2261 (2016).

87. De Lavergne, C., Madec, G., Roquet, F., Holmes, R. M. & McDougall, T. J. Abyssal ocean overturning shaped by seafloor distribution. *Nature* **551**, 181–186 (2017).

88. Haertel, P. & Fedorov, A. The ventilated ocean. *J. Phys. Oceanogr.* **42**, 141 – 164 (2012).

89. Barkan, R., Winters, K. B. & Smith, S. G. L. Rotating horizontal convection. *J. Fluid Mech.* **723**, 556–586 (2013).

90. Klocker, A., Munday, D., Gayen, B., Roquet, F. & LaCasce, J. H. Deep-reaching global ocean overturning circulation generated by surface buoyancy forcing. *Tellus A Dyn. Meteorol. Oceanogr.* **75**, 392–409 (2023).

91. Vallis, G. K. Large-scale circulation and production of stratification: effects of wind, geometry, and diffusion. *J. Phys. Oceanogr.* **30**, 933–954 (2000).

92. Viebahn, J. P., von der Heydt, A. S., Le Bars, D. & Dijkstra, H. A. Effects of drake passage on a strongly eddying global ocean. *Paleoceanography* **31**, 564–581 (2016).

93. Zhang, Y. et al. Early Eocene vigorous ocean overturning and its contribution to a warm Southern Ocean. *Climate* **16**, 1263–1283 (2020).

94. Zhang, Y. et al. Early eocene ocean meridional overturning circulation: the roles of atmospheric forcing and strait geometry. *Paleoceanogr. Paleoclimatol.* **37**, e2021PA004329 (2022).

95. Samelson, R. & Vallis, G. Large-scale circulation with small diapycnal diffusion: the two-thermocline limit. *J. Mar. Res.* **55**, https://elischolar.library.yale.edu/journal_of_marine_research/2224 (1997).

96. Richter, D. H. & Veron, F. Ocean spray: an outsized influence on weather and climate. *Phys. Today* **69**, 34–39 (2016).

97. Bhagtani, D., Hogg, A. M., Holmes, R. M. & Constantinou, N. C. Surface heating steers planetary-scale ocean circulation. *J. Phys. Oceanogr.* **53**, 2375–2391 (2023).

98. Luyten, J., Pedlosky, J. & Stommel, H. The ventilated thermocline. *J. Phys. Oceanogr.* **13**, 292–309 (1983).

99. Huang, R. X. On boundary value problems of the ideal-fluid thermocline. *J. Phys. Oceanogr.* **18**, 619–641 (1988).

100. Newsom, E. R. & Thompson, A. F. Reassessing the role of the indo-pacific in the ocean's global overturning circulation. *Geophys. Res. Lett.* **45**, 12–422 (2018).

101. Talley, L. D. Shallow, intermediate and deep overturning components of the global heat budget. *J. Phys. Oceangr.* **33**, 530–560 (2003).

102. Ferrari, R. & Ferreira, D. What processes drive the ocean heat transport? *Ocean Model.* **38**, 171–186 (2011).

103. Lenn, Y.-D. & Chereskin, T. K. Observations of Ekman currents in the Southern Ocean. *J. Phys. Oceanogr.* **39**, 768–779 (2009).

104. Ito, T., Marshall, J. & Follows, M. What controls the uptake of transient tracers in the Southern Ocean? *Glob. Biogeochem. Cycles* **18**, https://doi.org/10.1029/2003GB002103 (2004).

105. Marshall, D. Subduction of water masses in an eddying ocean. *J. Mar. Res.* **55**, 201–222 (1997).

106. Marshall, J. & Radko, T. Residual-mean solutions for the antarctic circumpolar current and its associated overturning circulation. *J. Phys. Oceanogr.* **33**, 2341–2354 (2003).

107. Karsten, R. H. & Marshall, J. Constructing the residual circulation of the ACC from observations. *J. Phys. Oceanogr.* **32**, 3315–3327 (2002).

108. Wolfe, C. L. & Cessi, P. The adiabatic pole-to-pole overturning circulation. *J. Phys. Oceanogr.* **41**, 1795–1810 (2011).

109. Nikurashin, M. & Vallis, G. A theory of the interhemispheric meridional overturning circulation and associated stratification. *J. Phys. Oceanogr.* **42**, 1652–1667 (2012).

110. Rousselet, L., Cessi, P. & Forget, G. Coupling of the mid-depth and abyssal components of the global overturning circulation according to a state estimate. *Sci. Adv.* **7**, eabf5478 (2021).

111. Rousselet, L. & Cessi, P. Diabatic transformations along the global routes of the middepth meridional overturning circulation. *J. Phys. Oceanogr.* **52**, 3159–3177 (2022).

112. Baker, J. A. et al. Overturning pathways control AMOC weakening in CMIP6 models. *Geophys. Res. Lett.* **50**, e2023GL103381 (2023).

113. Baker, J. A., Watson, A. J. & Vallis, G. K. Meridional overturning circulation in a multibasin model. Part II: sensitivity to diffusivity and wind in warm and cool climates. *J. Phys. Oceanogr.* **51**, 1813–1828 (2021).

114. Gnanadesikan, A. A simple predictive model for the structure of the oceanic pycnocline. *Science* **283**, 2077–2079 (1999).

115. Shakespeare, C. J. & McC. Hogg, A. An analytical model of the response of the meridional overturning circulation to changes in wind and buoyancy forcing. *J. Phys. Oceanogr.* **42**, 1270–1287 (2012).

116. Ferrari, R., Nadeau, L.-P., Marshall, D. P., Allison, L. C. & Johnson, H. L. A model of the ocean overturning circulation with two closed basins and a reentrant channel. *J. Phys. Oceanogr.* **47**, 2887–2906 (2018).

117. Adkins, J. F., McIntyre, K. & Schrag, D. P. The salinity, temperature, and δ18O of the glacial deep ocean. *Science* **298**, 1769–1773 (2002).

118. Hallberg, R. & Gnanadesikan, A. The role of eddies in determining the structure and response of the wind-driven southern hemisphere overturning: results from the modeling eddies in the southern ocean (meso) project. *J. Phys. Oceanogr.* **36**, 2232–2252 (2006).

119. Abernathey, R., Marshall, J. & Ferreira, D. The dependence of southern ocean meridional overturning on wind stress. *J. Phys. Oceanogr.* **41**, 2261–2278 (2011).

120. Marshall, D. P., Ambaum, M. H. P., Maddison, J. R., Munday, D. R. & Novak, L. Eddy saturation and frictional control of the Antarctic Circumpolar Current. *Geophys. Res. Lett.* **44**, 286–292 (2017).

121. Gent, P. R. Effects of southern hemisphere wind changes on the meridional overturning circulation in ocean models. *Annu. Rev. Mar. Sci.* **8**, 79–94 (2016).

122. Bishop, S. P. et al. Southern ocean overturning compensation in an eddy-resolving climate simulation. *J. Phys. Oceanogr.* **46**, 1575–1592 (2016).

123. Mak, J., Marshall, D. P., Madec, G. & Maddison, J. R. Acute sensitivity of global ocean circulation and heat content to eddy energy dissipation timescale. *Geophys. Res. Lett.* **49**, e2021GL097259 (2022).

124. Stommel, H. Thermohaline convection with two stable regimes of flow. *Tellus* **13**, 224–230 (1961).

125. Johnson, H., Marshall, D. & Sproson, D. Reconciling theories of a mechanically driven Meridional Overturning Circulation with thermohaline forcing and multiple equilibria. *Clim. Dyn.* **29**, 821–836 (2007).

126. Lynch-Stieglitz, J. The Atlantic meridional overturning circulation and abrupt climate change. *Annu. Rev. Mar. Sci.* **9**, 83–104 (2021).

127. Baker, J. A. et al. Continued Atlantic overturning circulation even under climate extremes. *Nature* **638**, 987–994 (2025).

128. van Westen, R. M. & Dijkstra, H. A. Asymmetry of amoc hysteresis in a state-of-the-art global climate model. *Geophys. Res. Lett.* **50**, e2023GL106088 (2023).

129. Roquet, F., Ferreira, D., Caneill, R., Schlesinger, D. & Madec, G. Unique thermal expansion properties of water key to the formation of sea ice on Earth. *Sci. Adv.* **8**, https://doi.org/10.1126/sciadv.abq0793 (2022).

130. Nycander, J., Hieronymus, M. & Roquet, F. The nonlinear equation of state of sea water and the global water mass distribution. *Geophys. Res. Lett.* **42**, 7714–7721 (2015).

131. Groeskamp, S., Abernathey, R. P. & Klocker, A. Water mass transformation by cabbeling and thermobaricity. *Geophys. Res. Lett.* **43**, 10–835 (2016).

132. Caneill, R., Roquet, F., Madec, G. & Nycander, J. The polar transition from alpha to beta regions set by a surface buoyancy flux inversion. *J. Phys. Oceanogr.* **52**, 1887–1902 (2022).

133. Winton, M. The effect of cold climate upon north Atlantic deep water formation in a simple ocean-atmosphere model. *J. Clim.* **10**, 37–51 (1997).

134. de Boer, A. M., Sigman, D. M., Toggweiler, J. R. & Russell, J. L. Effect of global ocean temperature change on deep ocean ventilation. *Paleoceanography* **22**, https://doi.org/10.1029/2005PA001242; https://onlinelibrary.wiley.com/doi/pdf/10.1029/2005PA001242 (2007).

135. Sigman, D. M., Jaccard, S. L. & Haug, G. H. Polar ocean stratification in a cold climate. *Nature* **428**, 59–63 (2004).

136. Scher, H. D. & Martin, E. E. Timing and climatic consequences of the opening of Drake passage. *Science* **312**, 428–430 (2006).

137. Toggweiler, J. R. & Samuels, B. Effect of Drake passage on the global thermohaline circulation. *Deep Sea Res. Part I Oceanogr. Res. Pap.* **42**, 477–500 (1995).

138. Ferreira, D. et al. Atlantic-Pacific asymmetry in deep water formation. *Annu. Rev. Earth Planet. Sci.* **46**, 327–352 (2018).

139. Liu, W. & Hu, A. The role of the PMOC in modulating the deglacial shift of the ITCZ. *Clim. Dyn.* **45**, 3019–3034 (2015).

140. Thomas, D. J., Korty, R., Huber, M., Schubert, J. A. & Haines, B. Nd isotopic structure of the Pacific Ocean 70-30 Ma and numerical evidence for vigorous ocean circulation and ocean heat transport in a greenhouse world. *Paleoceanography* **29**, 454–469 (2014).

141. Waddell, L. M. & Moore, T. C. Salinity of the Eocene Arctic Ocean from oxygen isotope analysis of fish bone carbonate. *Paleoceanography* **23**, https://doi.org/10.1029/2007PA001451 (2008).

142. Hutchinson, D. K. et al. Arctic closure as a trigger for Atlantic overturning at the Eocene-Oligocene Transition. *Nat. Commun.* **10**, 3797 (2019).

143. Pillot, Q., Donnadieu, Y., Sarr, A.-C., Ladant, J.-B. & Suché ras Marx, B. Evolution of ocean circulation in the North Atlantic Ocean during the Miocene: impact of the greenland ice sheet and the Eastern Tethys Seaway. *Paleoceanogr. Paleoclimatol.* **37**, e2022PA004415 (2022).

144. Molnar, P. Closing of the Central American seaway and the ice age: a critical review. *Paleoceanography* **23**, https://doi.org/10.1029/2007PA001574 (2008).

145. Burton, K. W., Ling, H.-F. & O'Nions, R. K. Closure of the Central American Isthmus and its effect on deep-water formation in the North Atlantic. *Nature* **386**, 382–385 (1997).

146. Hamon, N., Sepulchre, P., Lefebvre, V. & Ramstein, G. The role of eastern Tethys seaway closure in the Middle Miocene Climatic Transition (ca. 14 Ma). *Climate* **9**, 2687–2702 (2013).

147. Bell, D. B. et al. Atlantic deep-water response to the early pliocene shoaling of the Central American seaway. *Sci. Rep.* **5**, 12252 (2015).

148. Hall, J. R., Allison, M. S., Papadopoulos, M. T., Barfod, D. N. & Jones, S. M. Timing and consequences of bering strait opening: new insights from 40Ar/39Ar dating of the Barmur Group (Tjörnes Beds), Northern Iceland. *Paleoceanogr. Paleoclimatol.* **38**, e2022PA004539 (2023).

149. Weiffenbach, J. E. et al. Unraveling the mechanisms and implications of a stronger mid-Pliocene Atlantic Meridional Overturning Circulation (AMOC) in PlioMIP2. *Climate* **19**, 61–85 (2023).

150. Yang, X. & Cessi, P. The bering strait throughflow component of the global mass, heat and freshwater transport. *J. Geophys. Res. Oceans* **129**, e2024JC021463 (2024).

151. De Boer, A. M. & Nof, D. The Bering Strait's grip on the northern hemisphere climate. *Deep Sea Res. Part I Oceanogr. Res. Pap.* **51**, 1347–1366 (2004).

152. Hu, A. & Meehl, G. A. Bering Strait throughflow and the thermohaline circulation. *Geophys. Res. Lett.* **32**, https://doi.org/10.1029/2005GL024424 (2005).

153. Hasumi, H. Sensitivity of the global thermohaline circulation to interbasin freshwater transport by the atmosphere and the Bering Strait throughflow. *J. Clim.* **15**, 2516–2526 (2002).

154. Jones, C. S. & Cessi, P. Size matters: another reason why the Atlantic is saltier than the Pacific. *J. Phys. Oceanogr.* **47**, 2843–2859 (2017).

155. Youngs, M. K., Ferrari, R. & Flierl, G. R. Basin-width dependence of northern deep convection. *Geophys. Res. Lett.* **47**, e2020GL089135 (2020).

156. Ragen, S., Armour, K. C., Thompson, L., Shao, A. & Darr, D. The role of Atlantic basin geometry in meridional overturning circulation. *J. Phys. Oceanogr.* **52**, 475–492 (2022).

157. Nilsson, J., Langen, P. L., Ferreira, D. & Marshall, J. Ocean basin geometry and the salinification of the Atlantic ocean. *J. Clim.* **26**, 6163–6184 (2013).

158. Green, J. A. M. et al. Tidal mixing and the meridional overturning circulation from the last glacial maximum. *Geophys. Res. Lett.* **36**, https://doi.org/10.1029/2009GL039309 (2009).

159. Green, J. A. M., Huber, M., Waltham, D., Buzan, J. & Wells, M. Explicitly modelled deep-time tidal dissipation and its implication for Lunar history. *Earth Planet. Sci. Lett.* **461**, 46–53 (2017).

160. Polzin, K. L., Speer, K. G., Toole, J. M. & Schmitt, R. W. Intense mixing of Antarctic bottom water in the equatorial Atlantic Ocean. *Nature* **380**, 54–57 (1996).

161. Bryden, H. L. & Nurser, A. J. G. Effects of strait mixing on ocean stratification. *J. Phys. Oceanogr.* **33**, 1870–1872 (2003).

162. St Laurent, L. C., Toole, J. M. & Schmitt, R. W. Buoyancy forcing by turbulence above rough topography in the Abyssal Brazil Basin. *J. Phys. Oceanogr.* **31**, 3476–3495 (2001).

163. Holzer, M., DeVries, T. & de Lavergne, C. Diffusion controls the ventilation of a Pacific Shadow Zone above abyssal overturning. *Nat. Commun.* **12**, 4348 (2021).

164. Maher, K. & Chamberlain, C. P. Hydrologic regulation of chemical weathering and the geologic carbon cycle. *Science* **343**, 1502–1504 (2014).

165. Elsworth, G., Galbraith, E., Halverson, G. & Yang, S. Enhanced weathering and CO2 drawdown caused by latest Eocene strengthening of the Atlantic meridional overturning circulation. *Nat. Geosci.* **10**, 213–216 (2017).

166. Schmittner, A., Silva, T. A. M., Fraedrich, K., Kirk, E. & Lunkeit, F. Effects of mountains and ice sheets on global ocean circulation. *J. Clim.* **24**, 2814–2829 (2011).

167. Maffre, P., Ladant, J.-B., Donnadieu, Y., Sepulchre, P. & Goddéris, Y. The influence of orography on modern ocean circulation. *Clim. Dyn.* **50**, 1277–1289 (2018).

168. Sinha, B. et al. Mountain ranges favour vigorous Atlantic meridional overturning. *Geophys. Res. Lett.* **39**, https://doi.org/10.1029/2011GL050485 (2012).

169. Hirschi, J. J.-M. et al. The atlantic meridional overturning circulation in high-resolution models. *J. Geophys. Res. Oceans* **125**, e2019JC015522 (2020).

170. Roberts, M. J. et al. Sensitivity of the Atlantic meridional overturning circulation to model resolution in CMIP6 HighResMIP simulations and implications for future changes. *J. Adv. Model. Earth Syst.* **12**, e2019MS002014 (2020).

171. Jackson, L. C. et al. Impact of ocean resolution and mean state on the rate of AMOC weakening. *Clim. Dyn.* **55**, 1711–1732 (2020).

172. Sherriff-Tadano, S. et al. Southern ocean surface temperatures and cloud biases in climate models connected to the representation of glacial deep ocean circulation. *J. Clim.* **36**, 3849–3866 (2023).

173. Liu, W., Xie, S.-P., Liu, Z. & Zhu, J. Overlooked possibility of a collapsed Atlantic meridional overturning circulation in warming climate. *Sci. Adv.* **3**, e1601666 (2017).

174. Bonan, D. B. et al. Observational constraints imply limited future Atlantic meridional overturning circulation weakening. *Nat. Geosci.* **18**, 479–487 (2025).

175. Pavia, F. J., Jones, C. S. & Hines, S. K. Geometry of the meridional overturning circulation at the last glacial maximum. *J. Clim.* **35**, 5465–5482 (2022).

176. Held, I. M. et al. Probing the fast and slow components of global warming by returning abruptly to preindustrial forcing. *J. Clim.* **23**, 2418–2427 (2014).

177. Frölicher, T. L. et al. Dominance of the Southern Ocean in anthropogenic carbon and heat uptake in CMIP5 models. *J. Clim.* **28**, 862–886 (2015).

178. Bernardello, R. et al. Response of the ocean natural carbon storage to projected twenty-first-century climate change. *J. Clim.* **27**, 2033–2053 (2014).

179. Ödalen, M., Nycander, J., Oliver, K. I. C., Brodeau, L. & Ridgwell, A. The influence of the ocean circulation state on ocean carbon storage and CO2 drawdown potential in an Earth system model. *Biogeosciences* **15**, 1367–1393 (2018).

180. Archer, D. et al. Atmospheric lifetime of fossil fuel carbon dioxide. *Annu. Rev. Earth Planet. Sci.* **37**, 117–134 (2009).

181. Olson, S. L., Jansen, M. & Abbot, D. S. Oceanographic considerations for exoplanet life detection. *Astrophys. J.* **895**, 19 (2020).

182. Srinivasan, M. & Tsontos, V. Satellite altimetry for ocean and coastal applications: a review. *Remote Sens.* **15**, 3939 (2023).

183. Weller, R. A. et al. The challenge of sustaining ocean observations. *Front. Mar. Sci.* **6**, https://doi.org/10.3389/fmars.2019.00105 (2019).

184. Wunsch, C., Schmitt, R. W. & Baker, D. J. Climate change as an intergenerational problem. *Proc. Natl. Acad. Sci. USA* **110**, 4435–4436 (2013).

185. Lumpkin, R. & Speer, K. Global ocean meridional overturning. *J. Phys. Oceanogr.* **37**, 2550–2562 (2007).

186. Talley, L. D. Closure of the global overturning circulation through the Indian, Pacific, and Southern oceans: schematics and transports. *Oceanography* **26**, 80–97 (2013).

187. Lu, P., McCreary, J. P. & Klinger, B. A. Meridional circulation cells and the source waters of the Pacific equatorial undercurrent. *J. Phys. Oceanogr.* **28**, 62–84 (1998).

188. Forget, G. & Ferreira, D. Global ocean heat transport dominated by heat export from the tropical Pacific. *Nat. Geosci.* **12**, 351 (2019).

189. Monkman, T. & Jansen, M. F. The global overturning circulation and the role of non-equilibrium effects in ECCOv4r4. *J. Geophys. Res. Oceans* **129**, e2023JC019690 (2024).

190. Young, W. R. Dynamic Enthalpy, conservative temperature, and the seawater boussinesq approximation. *J. Phys. Oceanogr.* **40**, 394–400 (2010).

191. Nycander, J. Energy conversion, mixing energy, and neutral surfaces with a nonlinear equation of state. *J. Phys. Oceanogr.* **41**, 28–41 (2011).

192. McDougall, T. J. & McIntosh, P. C. The temporal-residual-mean velocity. Part II: isopycnal interpretation and the tracer and momentum equations. *J. Phys. Oceanogr.* **31**, 1222–1246 (2001).

193. Kamm, D., Deshayes, J. & Madec, G. DINO: a diabatic model of pole-to-pole ocean dynamics to assess subgrid parameterizations across horizontal scales. *EGUsphere* 1–26, https://doi.org/10.5194/egusphere-2025-1100 (2025).

194. Häfner, D., Nuterman, R. & Jochum, M. Fast, cheap, and turbulent—global ocean modeling with GPU acceleration in Python. *J. Adv. Model. Earth Syst.* **13**, e2021MS002717 (2021).

195. Bryan, K. & Lewis, L. J. A water mass model of the World Ocean. *J. Geophys. Res. Oceans* **84**, 2503–2517 (1979).

196. Zaucker, F. & Broecker, W. S. The influence of atmospheric moisture transport on the fresh water balance of the Atlantic drainage basin: general circulation model simulations and observations. *J. Geophys. Res. Atmos.* **97**, 2765–2773 (1992).

197. Craig, P. M., Ferreira, D. & Methven, J. Monsoon-induced zonal asymmetries in moisture transport cause anomalous pacific precipitation minus evaporation. *Geophys. Res. Lett.* **47**, e2020GL088659 (2020).

198. Su, B., Jiang, D., Zhang, R., Sepulchre, P. & Ramstein, G. Difference between the North Atlantic and Pacific meridional overturning circulation in response to the uplift of the Tibetan Plateau. *Climate* **14**, 751–762 (2018).

199. Polzin, K. L., Toole, J. M., Ledwell, J. R. & Schmitt, R. W. Spatial variability of turbulent mixing in the abyssal ocean. *Science* **276**, 93–96 (1997).

200. Klymak, J. M. Nonpropagating form drag and turbulence due to stratified flow over large-scale abyssal hill topography. *J. Phys. Oceanogr.* **48**, 2383–2395 (2018).

201. Egbert, G. D., Ray, R. D. & Bills, B. G. Numerical modeling of the global semidiurnal tide in the present day and in the last glacial maximum. *J. Geophys. Res. Oceans* **109**, https://doi.org/10.1029/2003JC001973 (2004).

Author contributions
F.R. led the development of the paper, with special assistance from M.B. F.R. produced Figs. 1, 2, 5, 7 and 10. C.S.J. produced Figs. 3 and 8. J.N. and F.R. produced Fig. 4. J.L.C. produced Fig. 6, adapted from Gjermundsen and LaCasce[67]. D.P.M. produced Fig. 9 with help from A.d.B., C.d.L. and M.O. Every authors contributed to the writing and reviewed the manuscript.

Competing interests
The authors declare no competing interests.

Additional information
Correspondence and requests for materials should be addressed to Fabien Roquet.

Reprints and permissions information is available at http://www.nature.com/reprints

Publisher's note Springer Nature remains neutral with regard to jurisdictional claims in published maps and institutional affiliations.